

Article

Investigating Scale Effects on Experimental Shear Strength of Earthen Walls (Adobe and Rammed-Earth)

Daniel M. Ruiz ^{1,*}, Juan C. Reyes ², Yezid A. Alvarado ¹, Hermes Vacca ¹, Nicola Tarque ³
and Sandra Jerez ⁴

¹ Department of Civil Engineering, Pontificia Universidad Javeriana, Carrera 7 No. 40-62, Bogotá 110231, Colombia; alvarado.y@javeriana.edu.co (Y.A.A.); vacca@javeriana.edu.co (H.V.)

² Department of Civil and Environmental Engineering, Universidad de Los Andes, Carrera 1 No. 18A-12, Bogotá 111711, Colombia; jureyes@uniandes.edu.co

³ Department of Continuum Mechanics and Structures, Universidad Politécnica de Madrid, 28040 Madrid, Spain; nicola.tarque@upm.es

⁴ Center for the Study of Structures, Materials and Construction, Universidad Escuela Colombiana de Ingeniería, Autopista Norte AK 45 No. 205-59, Bogotá 111321, Colombia; sandra.jerez@escuelaing.edu.co

* Correspondence: daniel.ruiz@javeriana.edu.co

Abstract: This study investigates the scale effects on the experimental shear strength of earthen walls, a critical parameter influencing the seismic performance of adobe and rammed-earth (RE) buildings. Recognized for their historical significance and sustainable construction practices, earthen structures require a comprehensive understanding of their mechanical behavior under shear loads to ensure effective design and preservation. This research compiles data from over 120 in-plane shear wall tests (adobe and RE), nearly 20 direct shear tests from the scientific and technical literature, and new cyclic direct shear tests performed on large cubic specimens (300 mm side length) made from the same material as a previously tested two-story RE wall. Based on the findings, this study recommends a minimum specimen cross-sectional area of 0.5 m² for reliable shear strength testing of earthen walls in structural laboratories. This recommendation aims to prevent the unconservative overestimation of shear strength commonly observed in smaller specimens, including direct shear tests. Furthermore, the Mohr–Coulomb failure criterion outlined in the AIS-610 Colombian standard is validated as a conservative lower bound for all compiled shear strength data. Cyclic direct shear tests on nine 300 mm cubic specimens produced a Mohr–Coulomb envelope with an apparent cohesion of 0.0715 MPa and a slope of 0.66, whereas the full-scale two-story wall (5.95 × 6.20 × 0.65 m) constructed with the same material exhibited a much lower cohesion of 0.0139 MPa and a slope of 0.26. The analysis reveals significant scale effects, as small-scale specimens consistently overestimate shear strength due to their inability to capture macro-structural behaviors such as compaction layer interactions, construction joint weaknesses, and stress redistributions. Based on the analysis of the compiled data, the novelty of this study lies in defining a strength reduction factor for direct shear tests (3.4–3.8 for rammed earth, ~3.0 for adobe) to align with full-scale wall behavior, as well as establishing a minimum specimen size (≥ 0.5 m²) for reliable in-plane shear testing of earthen walls, ensuring accurate structural assessments of shear strength. This study provides a first approach to the shear behavior of unstabilized earth. To expand its application, future research should explore how the scale of specimens with different stabilizers affects their shear strength.

Keywords: shear strength; rammed-earth walls; adobe walls; direct shear tests; static and pseudo-static in-plane load shear tests



Academic Editors: Omar AlShawa, Stefania Degli Abbati and Giacomo Destro Bisol

Received: 26 January 2025

Revised: 14 February 2025

Accepted: 17 February 2025

Published: 22 February 2025

Citation: Ruiz, D.M.; Reyes, J.C.; Alvarado, Y.A.; Vacca, H.; Tarque, N.; Jerez, S. Investigating Scale Effects on Experimental Shear Strength of Earthen Walls (Adobe and Rammed-Earth). *Buildings* **2025**, *15*, 689. <https://doi.org/10.3390/buildings15050689>

Copyright: © 2025 by the authors. Licensee MDPI, Basel, Switzerland. This article is an open access article distributed under the terms and conditions of the Creative Commons Attribution (CC BY) license (<https://creativecommons.org/licenses/by/4.0/>).

1. Introduction

Earthen constructions have been fundamental to architectural and cultural heritage for centuries. Found across continents, these structures exemplify the effective use of locally sourced building materials that are among the oldest and most commonly utilized (with their use dating back to as early as 8000 B.C. [1]) to create durable and functional buildings. These earthen buildings demonstrate the technical expertise and craftsmanship of ancient civilizations, as illustrated by sites such as Çatalhöyük in Turkey, Chan Chan in Peru, Muslim fortresses in Spain and North Africa, Buddhist monasteries in India, colonial constructions in the historic centers of Colombian cities, and traditional dwellings across various regions of Peru [2–4]. The historical value of earthen buildings, combined with their adaptability to local conditions, underscores their role as a vital part of global heritage. Beyond their cultural significance, earthen constructions are renowned for their environmental benefits. Unlike conventional materials such as concrete and steel, earthen materials have substantially lower embodied energy, contributing to a reduced carbon footprint during construction [5,6]. Moreover, according to [7], earthen walls provide natural thermal insulation, helping to regulate indoor temperatures and reduce energy consumption for heating and cooling, while also offering favorable hygrothermal properties. These features align earthen construction techniques with modern sustainability goals, making them a practical and eco-friendly choice for contemporary building practices [8,9]. The natural biodegradability of earthen materials significantly reduces their environmental impact at the end of their lifecycle, enhancing their ecological attractiveness.

Construction techniques such as adobe, rammed earth (RE), and bahareque continue to be widely used due to their inherent sustainability and cost-effectiveness. Adobe is created by molding a mixture of soil, water, and organic fibers into blocks, which are then air-dried. In contrast, RE involves the construction of large earthen blocks by compacting layers of moist soil [10,11]. Reference [12] defines the bahareque system (Quincha in Peru) as a lightweight durable framework, typically made of bamboo (known as guadua in Colombia) or wood, which is filled with a soil-based mixture. These techniques, deeply rooted in local traditions, have retained their relevance across diverse regions worldwide [5]. The structural performance of these materials, however, is subject to key factors, including material composition, compaction methodology, the use of chemical stabilizers [13], and curing conditions. These parameters exhibit substantial variability depending on regional practices and environmental conditions, resulting in differences in mechanical properties and performance. However, the seismic behavior of earthen walls remains a critical concern due to the prevalence of these constructions in earthquake-prone regions. Earthen walls frequently exhibit poor seismic performance due to their inherent material properties and construction methods. Key factors contributing to the seismic vulnerability of adobe and RE structures include irregularities in plan and elevation, insufficient wall distribution, moisture-related issues, weak or inadequate wall-to-wall connections, and their inherently low tensile and shear strength [14]. The collapse of earthen buildings in past earthquakes has exposed their structural weaknesses, emphasizing the urgent need for improved construction practices and effective retrofitting strategies [15,16]. Notable seismic events have demonstrated the poor performance of earthen buildings, including the 2007 Peru earthquake ($M_w = \text{Moment Weight} = 8.0$), the 2010 Chile earthquake ($M_w 8.8$), the 2003 Iran earthquake ($M_w 6.6$), and the 1992 Turkey earthquake ($M_w 6.8$). In Colombia, earthquakes have similarly impacted historic earthen constructions, as observed during the 1999 Coffee-Growing Region earthquake ($M_w 6.2$), the 1983 Popayán earthquake ($M_w 5.5$), and the 1875 Cúcuta earthquake ($M_w 7.5$) [2,11,17,18]. Structural failures in RE and adobe constructions during seismic events are frequently attributed to poor shear and tensile strength, leading to diagonal cracking and cracking along construction joints [19–22].

Understanding the mechanical behavior of earthen walls, particularly their shear strength, is essential for ensuring their safety, stability, and long-term resilience in seismic regions. However, due to limitations in research resources and structural laboratory capacities, most studies on the shear strength of earthen walls have focused on reduced-scale models of individual walls, with relatively few involving full-scale and large wall specimens. This research gap highlights the urgent need for more comprehensive experimental programs (like the research performed in [11,23] to improve our understanding of full-scale earthen walls' behavior under seismic loading.

The objectives and novelty of this study lie in its comprehensive integration and comparison of in-plane shear tests of earthen walls with direct shear tests, providing critical insights into the mechanical behavior of RE and adobe walls. Unlike previous studies, which typically focused on either small-scale shear tests or isolated wall tests, this research is the first to systematically integrate direct shear tests with in-plane shear tests on earthen walls, including those with openings such as doors and windows. This approach allows for a direct comparison of shear strength values at different scales, addressing a significant gap in the literature. By synthesizing and analyzing data from both methodologies, this research enhances the understanding of how specimen scale influences shear strength and failure mechanisms. This study aims to (1) quantify the relationship between structural element size and shear strength, highlighting distinct differences in strength characteristics between full-scale and smaller specimens, including the effect of axial stress; and to (2) define minimum specimen sizes for reliable shear strength estimation and propose a strength reduction factor to align direct shear test results with wall behavior. The findings have significant practical implications for the seismic assessment, design, and construction of RE and adobe structures, particularly in regions that are prone to earthquakes. This study provides specific recommendations for the minimum specimen sizes needed to obtain accurate shear strength estimates and ensure reliable data for structural analysis. Furthermore, our results contribute to the refinement of building codes, supporting the safer and more efficient application of earthen construction techniques in modern architectural and engineering practices.

2. Methodology

Figure 1 presents the methodology used in this study, which consisted of five distinct phases:

- Phase 1: Collecting data from in-plane shear load tests on walls. The initial phase of this research entailed the collection of data from 125 experimental in-plane shear load tests on earthen walls, as documented in scientific journal articles and conference papers. These tests were selected based on their availability in the literature rather than a predefined experimental design. The selection criteria included studies reporting pseudo-static or cyclic loading tests on walls or wall segments, ensuring relevance to this study's objectives. The dataset was compiled by extracting numerical values (e.g., dimensions, axial forces/stresses, shear forces/stresses, etc.) directly from tables and text descriptions in the original documents. In cases where the results were only available as force–displacement curves, the data were digitized to obtain key parameters. This extensive dataset formed the basis for subsequent analyses. A comprehensive statistical analysis was conducted to identify trends and patterns in shear strength behavior, ensuring that the findings reflected the structural response of earthen walls under in-plane shear loads. Furthermore, a detailed examination of the relationship between specimen size and shear strength was performed to evaluate the impact of scale on mechanical properties. Using the compiled results, Mohr–Coulomb failure envelopes were derived, yielding critical parameters such as cohesion and

internal friction angle based on the observed axial stress (σ) vs. shear strength (τ) data in the tests.

- Phase 2: Compiling monotonic direct shear tests and failure surfaces for Mohr–Coulomb properties. This phase involved compiling 22 monotonic direct shear tests (or models) from the scientific and technical literature, including 19 tests (models) performed with axial loading and 3 tests conducted without axial loading. These tests were selected based on their availability in the literature rather than a predefined experimental design. Also, these tests were analyzed, providing additional insights into material behavior under shear loading conditions. The collected data, as detailed in the table in Section 3.2, included key parameters related to the Mohr–Coulomb failure surface, such as regression slopes (associated with the friction angle) and intercepts (corresponding to cohesion). In cases where specific parameters were not directly reported, they were derived from the available numerical data or extracted through digitalization of force–displacement and stress–strain curves.
- Phase 3: Conducting cyclic direct shear tests. This phase involved cyclic direct shear tests to assess the behavior of RE materials under repeated loading conditions, analogous to seismic demands. As presented in Section 4, the cyclic direct shear tests incorporated recommendations from international standards to ensure consistent displacement-controlled cyclic loading. The selected axial stress levels (24 kPa, 79 kPa, and 184 kPa) were chosen to represent typical working stresses in earthen buildings ranging from one to three stories. The direct shear tests in this study were performed on specimens larger than those traditionally used—specifically, cubic specimens with a side length of 300 mm. These experiments provided critical insights into the strength and energy dissipation behavior of RE under cyclic loading across various axial stress levels. Specimen preparation followed the same material composition, compaction layers (7.5–10 cm), and curing conditions as those used in previous full-scale wall tests conducted by some of the authors. These walls represent some of the largest earthen structures ever tested in structural laboratories globally, as documented in [11,23]. This comparative analysis validated the consistency of findings across different testing methods and scales.
- Phase 4: Comparing axial stress (σ) vs. shear strength (τ) data from different sources. The fourth phase focused on an integrated comparison of σ vs. τ data obtained from three key sources: in-plane shear tests on earthen walls (full-scale wall tests and wall tests), direct shear tests documented in the scientific and technical literature, and cyclic direct shear tests performed in this study. By synthesizing findings across these datasets, our research offered a unified perspective on the mechanical behavior of earthen walls under shear loading. This phase also underscored the critical role of specimen size and testing methodology in shaping observed failure mechanisms and strength parameters.
- Phase 5: Integrating results to obtain conclusions. The final phase synthesized the findings from all preceding phases to develop a comprehensive understanding of the mechanical behavior of earthen materials under shear loading. The analysis identified key trends and practical implications for the design and construction of earthen structures. Specific recommendations were made regarding the minimum specimen sizes required to reliably estimate actual shear strength. Also, the authors propose a strength reduction factor for direct shear tests to align them with the strength of full-scale earthen walls. Finally, our results offer guidance on incorporating σ vs. τ Mohr–Coulomb surfaces into building codes to improve their applicability and accuracy.

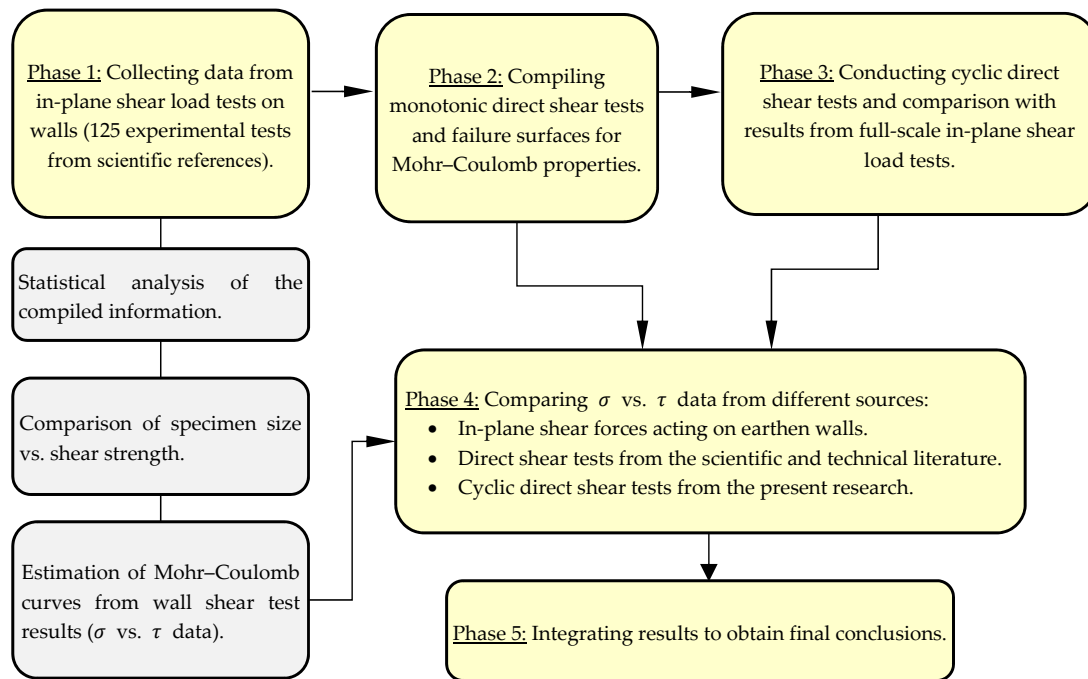


Figure 1. Proposed methodology to assess the shear strength of earthen walls (adobe and RE).

It is essential to clarify that, in this study, the term “small-scale” refers to direct shear test specimens, including cubic or prismatic samples, as well as small wall segments that do not represent complete structural elements. Conversely, “full-scale” describes large earthen walls tested under in-plane shear loads, with dimensions comparable to those found in real adobe or rammed-earth buildings. These walls possess representative lengths, heights, and thicknesses, enabling a realistic evaluation of shear strength at a structural level. In some cases, they also include openings such as doors or windows. While some tested walls meet the criteria for “full-scale”, others are simply referred to as “walls” when their dimensions do not fully correspond to those of real structures.

3. Database and Comparisons with Previous Research: In-Plane Shear Tests of Walls, and Direct Shear Tests

3.1. Collected Database: In-Plane Shear Load Tests from the Literature

Research on the seismic performance and shear resistance of adobe and RE walls has increasingly underscored the critical importance of in-plane load testing for accurately evaluating shear strength, particularly under static and pseudo-static loading conditions, in order to establish how earthen materials respond to lateral forces. For instance, Ref. [24] analyzed the in-plane lateral behavior of adobe walls under varying levels of axial compression, observing that lateral resistance significantly increased as the vertical compression stress rose from 0.1 to 0.7 MPa. Similarly, Ref. [25] employed scaled shaking table tests on scaled adobe wall models, highlighting their substantial vulnerability to shear-related failures in unreinforced conditions. The authors of ref. [26] showed that near-surface-mounted steel rebars effectively improved in-plane shear resistance in adobe walls by mitigating diagonal cracking tendencies. Reference [27] utilized biaxial loading (vertical/axial load and horizontal/shear load) on RE walls to examine shear failure patterns, highlighting the relationship between limit states and inter-story drifts for evaluating the seismic performance of earthen walls (limit states). Similarly, Ref. [28] observed that different types of adobe wall exhibited shear failure modes characterized by cracking along mud joints and oblique cracks propagating through the blocks. In a complementary study, Ref. [29]

conducted static pushover tests on RE walls to demonstrate how wall size influences both drift and in-plane shear resistance (different height/length ratios were tested with in-plane shear loads), providing a framework for understanding structural responses across varied configurations. Additionally, Ref. [30] investigated 1:2-scaled adobe walls under horizontal monotonic loading, identifying weak mortar bonds as a critical factor limiting shear capacity. This observation aligns with the findings from reference [31], where quasi-static tests on unreinforced adobe walls exhibited shear failure characterized by diagonal crack patterns along joints and through some adobe units. The tests reported in [31] on timber-reinforced adobe walls revealed substantial improvements in energy dissipation and shear strength, emphasizing the significant role of timber in enhancing deformation capacity and overall structural performance.

Heritage-focused studies contribute critical insights to shear testing research. For example, Ref. [32] examined pseudo-static shear behavior in adobe walls from heritage structures (doctrinal chapels), reporting early failure in unreinforced walls, while steel tensor reinforcement significantly improved their stability. Similarly, Ref. [19] investigated Bhutanese RE walls retrofitted with dowels, observing a 12.3% increase in shear resistance. One of Europe's largest full-scale adobe wall tests, reported in [33], involved a 5 m long and 3.6 m high wall under parallel-plane loading conditions. In Colombia, Refs. [11,23] performed the largest global full-scale parallel-plane shear tests on adobe and RE walls, establishing a benchmark for full-scale experimental studies. Specifically, Ref. [23] analyzed one-story, 7 m (length) adobe and RE walls, exploring both reinforced and unreinforced configurations. The results revealed limited shear strength and premature failure in unreinforced adobe walls under cyclic loading, whereas timber-reinforced walls exhibited significant enhancements in ductility and energy dissipation. For RE walls, Ref. [22] observed similar patterns, with brittle failure in unreinforced walls and substantial improvements in stability and crack resistance in reinforced walls.

At Pontificia Universidad Javeriana (Colombia, South America), Ref. [11] conducted the world's largest full-scale test on a two-story RE wall, measuring approximately 6 m in both length and height. Testing of the unreinforced wall highlighted the fragility of earthen constructions, demonstrating limited shear capacity, brittle failure, and a low drift at failure, close to 0.5%. After implementing a steel plate reinforcement system, Ref. [11] reported substantial performance improvements: cyclic shear tests revealed a 208% increase in lateral capacity, enhanced energy dissipation, and improved stability. This reinforcement method, incorporating horizontal and vertical steel plates, effectively confined the earthen material, minimized crack propagation, and significantly enhanced ductility within the wall plane. Similarly, Ref. [23] reported comparable benefits in one-story timber-reinforced earthen walls. The authors of [34,35] investigated the degradation of structural capacity in unstabilized RE and Portuguese adobe walls through in-plane shear tests under cyclic loading conditions.

Previously, Ref. [36] presented pushover tests to assess the shear–displacement behavior of RE walls with two height-to-length ratios, identifying nonlinear shear responses and underscoring the influence of material properties on structural performance. The tests shown in reference [37] revealed the fragile behavior of traditional Portuguese adobe walls subjected to horizontal shear in the laboratory, which is a problem for existing buildings in areas of moderate-to-high seismic hazard. The authors of [38] examined RE walls with structural columns, observing that these additions significantly enhanced shear strength under lateral loading. The research presented in [39] identified a trade-off in deformation capacity when utilizing geogrid sheets to improve shear resistance. Investigations into alternative reinforcement methods for earthen materials provide additional insights. For instance, Ref. [40] demonstrated that polyester strips enhance in-plane shear resistance in RE

walls under cyclic loading, while [41] identified three distinct failure modes in unreinforced earth walls: flexural cracking combined with diagonal shear, rocking with toe crushing and bed-joint sliding, and rocking accompanied by bed-joint failure. Similarly, Ref. [8] validated the effectiveness of mesh wraps in improving in-plane shear strength in RE wall elements, and ref. [9] highlighted the potential of sustainable palm mesh reinforcements to enhance shear resistance in adobe walls. Additionally, Ref. [42] pioneered the testing of cane mesh reinforcement in adobe walls under in-plane shear loads, emphasizing the importance of comprehensive testing to validate the shear response in retrofitted walls, underscoring the critical vulnerabilities of unreinforced walls in seismic conditions. In 1981 (in Peru), Ref. [43] conducted shear tests on adobe walls to evaluate in-plane shear resistance, emphasizing the importance of such testing for understanding adobe structures. Their findings revealed that reinforcements, such as cane, can enhance ductility and reduce failure risks, supporting safer construction practices for adobe buildings in seismic regions. The authors of [44] investigated the in-plane cyclic behavior of unfired clay and earthen brick walls, reporting significant shear strength improvements when reinforced with steel wire ropes and geo-net. Also, Ref. [45] proposed seismic retrofitting solutions using synthetic mesh for adobe walls, demonstrating considerable enhancements in the seismic performance. Finally, Ref. [46] demonstrated that the application of cold-formed thin-walled steel improved the seismic performance of adobe walls, as evidenced by increases in shear resistance (both cracking and ultimate load), ductility, and energy dissipation.

Complementarily, the studies reported in references [47,48] offer comparative evaluations of stabilized and unstabilized RE walls subjected to lateral cyclic loading, using lime or cement as stabilizers. Similarly, Refs. [10,49] highlight the advantages of externally bonded fiber reinforcements, which significantly enhance the shear resistance and displacement ductility capacity of earthen walls under seismic conditions. In addition, Ref. [50] combined experimental shear testing with finite element modeling to study the shear performance of adobe walls. Near-surface-mounted (NSM) reinforcement and sand-coated reeds (investigated by [51,52] showed a significant enhancement in the in-plane shear strength and seismic performance of adobe walls. Likewise, Ref. [53] investigated NSM retrofitting using reinforced mortar strips, bamboo plywood, and wood, reporting significant improvements in in-plane shear strength and lateral resistance, which are crucial for sustainable seismic retrofitting practices. The authors of [54] contributed to numerical modeling by developing adobe material parameters calibrated against quasi-static cyclic tests performed on adobe walls representative of Peruvian construction techniques. The authors of [55] investigated the behavior of RE walls in Eastern Europe (Croatia), analyzing key aspects such as shear stiffness degradation, load-bearing capacity, failure mechanisms, and energy dissipation. Finally, Ref. [56] studied adobe–brick composite walls reinforced with a wooden center column, demonstrating improved in-plane shear strength and resilience, making them suitable for rural construction applications.

Collectively, all of the aforementioned studies included in-plane shear tests on unstabilized/unreinforced walls (near-full-scale walls or full-scale walls), enabling comprehensive comparisons of shear resistance, ductility, energy dissipation, collapse mechanisms, and crack propagation between unreinforced and reinforced/strengthened walls. Based on the previous literature review, a comprehensive compilation of 125 tests on adobe and RE walls (unstabilized and un-strengthened) subjected to in-plane shear loads was conducted, incorporating both pseudo-static and monotonic testing methods. Some of these walls included openings, but the majority were solid walls without doors or windows. Figure 2 illustrates examples of two of the largest full-scale walls with openings tested in the consulted studies [11,23].

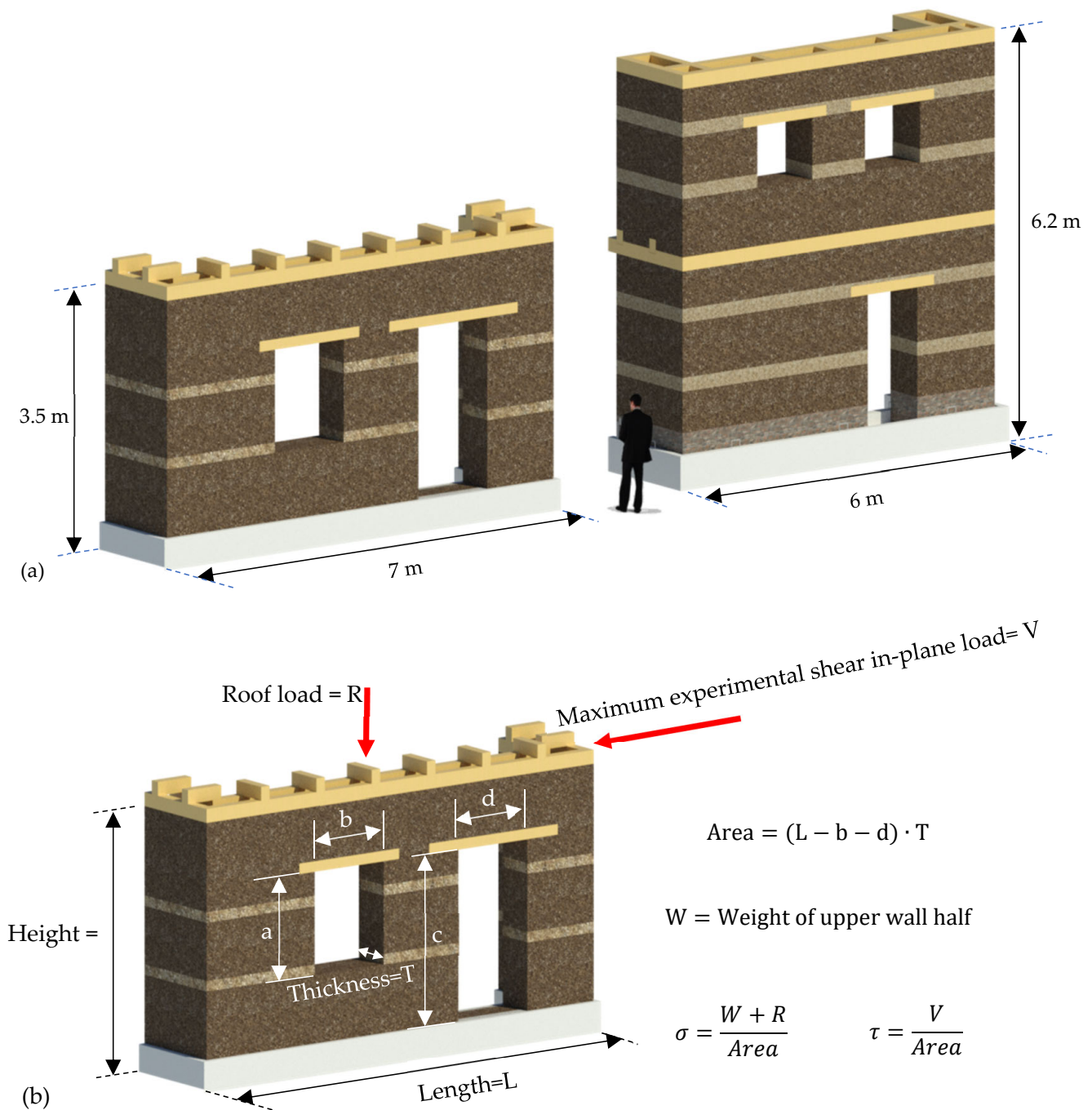


Figure 2. (a) Overall dimensions of two of the biggest walls with openings found in the references consulted (new schematic illustrations based on previous research [11,23]); (b) example of calculation of the axial stress (σ) and shear strength (τ) at mid-height of an earthen wall.

For each wall analyzed, the following parameters were compiled: the country where the tests were performed, presence or absence of openings, material type, unit weight, vertical roof load, wall dimensions (*Length*, *Height*, and *Thickness*), cross-sectional area at mid-height (*Area*), testing method (cyclic or monotonic), compressive strength of the material (f'_m), axial stress σ applied at mid-height, and shear strength τ at mid-height. The axial stress includes the weight of the upper half of the wall (W) and the roof load (R). Figure 2b shows an example of a one-story earthen wall with the geometric variables and the forces involved in the calculation of axial and shear stresses at mid-height. Table 1 summarizes the countries where most of these tests were performed, with Iran, Peru, Colombia, and China leading in contributions. Additionally, Tables 2 and 3 provide a

summary of the primary parameters involved in the in-plane shear tests, including data from 74 adobe wall tests (presented in Table 2) and 51 RE wall tests (presented in Table 3). A statistical analysis was conducted on the variables identified in the tests compiled in Tables 2 and 3. Frequency histograms, shown in Figure 3, were developed for geometric parameters such as wall length, wall height, wall thickness, slenderness ratio (length/thickness), and cross-sectional area. The analysis indicated that approximately 70% of the tested walls had a thickness of less than 0.33 m (Figure 3a), and the largest wall thickness tested was 0.65 m, as reported in [11]. The average slenderness ratio was close to 7.4 (Figure 3b). It is important to mention that recommendations for earthquake-resistant earthen walls suggest thicknesses ranging from 0.20 to 0.46 m [57]. This indicates that most investigations focus on thinner walls, likely due to the simplicity of the test setup, as testing thicker walls presents logistical challenges due to their size and weight. Additionally, the maximum slenderness ratio recommended for adequate seismic resistance, related to the maximum unsupported wall lengths, is approximately 10 [57]. Based on the statistical analysis in Figure 3b, over 70% of the walls tested under in-plane shear loads had slenderness ratios below 8.0, highlighting a tendency to test small walls, which may not fully represent real construction scenarios. Furthermore, only 30% of the collected data correspond to walls with heights greater than 2.2 m, which is likely the minimum standard for modern earthen buildings (Figure 3c). Additionally, Figure 3d shows that the average length of the walls tested was approximately 2.1 m.

Table 1. Countries where in-plane shear walls have been tested.

Country	Number of Wall Shear Tests
Iran	24
Peru	22
Colombia	21
China	20
France	13
Japan	11
Croatia	4
Germany	3
Portugal	3
Cyprus	1
Czech Republic	1
Italy	1
Turkey	1

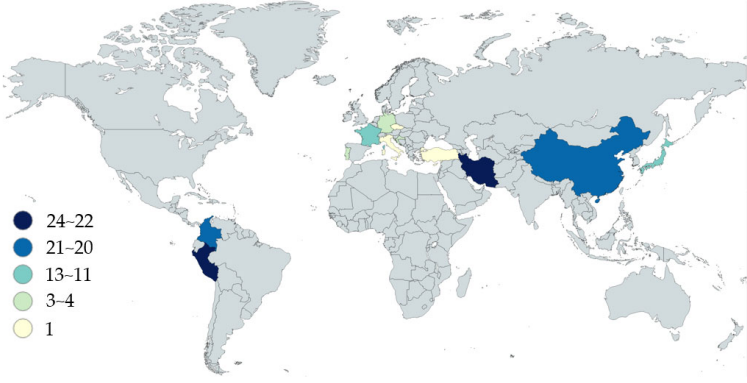


Table 2. Compilation of data from tests on adobe walls subjected to in-plane shear loads.

Openings	Unit Weight (kN/m ³)	Length (m)	Height (m)	Thickness (m)	Area (m ²)	Cyclic or Mono-tonic	Reference	f_m (MPa)	σ (MPa)	τ (MPa)
No	17.2	2.4	2.1	0.6	1.44	Cyclic	[10]	3.52	0.023	0.014
No	19.0 *	1.25	2.35	0.6	0.75	Cyclic	[16]	1.32	0.042	0.046
No	19.0 *	1.25	2.35	0.6	0.75	Cyclic	[16]	1.32	0.042	0.046
No	17.8	2.5	1.8	0.4	1	Cyclic	[22]	1.08	0.085	0.044
No	17.8	2.5	1.8	0.4	1	Cyclic	[22]	1.08	0.065	0.023
No	17.8	2.5	1.8	0.4	1	Cyclic	[22]	1.08	0.036	0.014
No	21.1	1.2	2.5	0.6	0.72	Cyclic	[22]	1.08	0.054	0.02
No	21.1	1.2	1.5	0.6	0.72	Cyclic	[22]	1.08	0.068	0.024
No	21.1	2.1	1.5	0.6	1.26	Cyclic	[22]	1.08	0.048	0.018
Yes	18.1	7	3.45	0.6	2.7	Cyclic	[23]	1.08	0.052	0.02
No	19.0 *	1	0.8	0.2	0.2	Cyclic	[24]	2.34	0.108	0.119

Table 2. Cont.

Openings	Unit Weight (kN/m ³)	Length (m)	Height (m)	Thickness (m)	Area (m ²)	Cyclic or Monotonic	Reference	f_m (MPa)	σ (MPa)	τ (MPa)
No	19.0 *	1	0.8	0.2	0.2	Cyclic	[24]	2.34	0.308	0.171
No	19.0 *	1	0.8	0.2	0.2	Cyclic	[24]	2.34	0.508	0.227
No	19.0 *	1	0.8	0.2	0.2	Cyclic	[24]	2.34	0.708	0.284
No	19.0 *	1	0.9	0.2	0.2	Cyclic	[24]	2.34	0.109	0.145
No	19.0 *	1	0.9	0.2	0.2	Cyclic	[24]	2.34	0.309	0.173
No	19.0 *	1	0.9	0.2	0.2	Cyclic	[24]	2.34	0.509	0.212
No	19.0 *	1	0.9	0.2	0.2	Cyclic	[24]	2.34	0.709	0.228
No	19.0 *	1	1	0.2	0.2	Cyclic	[24]	2.34	0.11	0.111
No	19.0 *	1	1	0.2	0.2	Cyclic	[24]	2.34	0.31	0.146
No	19.0 *	1	1	0.2	0.2	Cyclic	[24]	2.34	0.51	0.156
No	19.0 *	1	1	0.2	0.2	Cyclic	[24]	2.34	0.71	0.21
No	19.0 *	3.6	2.15	0.4	1.44	Cyclic	[25]	NA	0.022	0.025
Yes	19.0 *	3.6	2.15	0.4	1.04	Cyclic	[25]	NA	0.025	0.033
Yes	19.0 *	3.6	2.15	0.4	0.98	Cyclic	[25]	NA	0.025	0.031
No	19.0 *	1.02	0.8	0.2	0.204	Cyclic	[26]	2.34	0.108	0.105
No	19.0 *	1.02	0.8	0.2	0.204	Cyclic	[26]	2.34	0.308	0.142
No	19.0 *	1.7	1.1	0.24	0.41	Cyclic	[28]	0.87	0.11	0.086
Yes	19.0 *	1.75	1.58	0.22	0.26	Monotonic	[30]	NA	0.014	0.054
No	19.0 *	1.39	1.31	0.34	0.47	Cyclic	[31]	2	0.212	0.068
No	19.0 *	3.5	3	0.52	1.82	Cyclic	[32]	1.02	0.067	0.023
No	19.0 *	3.5	3	0.52	1.82	Cyclic	[32]	1.02	0.067	0.02
No	19.0 *	3.5	3	0.52	1.82	Cyclic	[32]	1.02	0.067	0.026
Yes	20	5.1	3.6	0.4	1.36	Cyclic	[33]	1.08	0.113	0.062
No	16	3.5	3.07	0.29	1.02	Cyclic	[37]	1.04	0.044	0.059
No	19.0 *	2	1.3	0.2	0.39	Cyclic	[41]	0.98	0.106	0.11
No	19.0 *	2	1.3	0.2	0.39	Cyclic	[41]	0.98	0.059	0.065
No	19.0 *	1.75	1.3	0.2	0.34	Cyclic	[41]	0.98	0.106	0.128
No	19.0 *	1.75	1.3	0.2	0.34	Cyclic	[41]	0.98	0.059	0.078
No	19.0 *	1.65	1.3	0.2	0.32	Cyclic	[41]	0.98	0.012	0.025
No	17.5	2.4	2.4	0.2	0.48	Monotonic	[42]	0.83	0.021	0.033
No	17.5	2.4	2.4	0.2	0.48	Monotonic	[42]	0.83	0.021	0.026
No	17.5	2.4	2.4	0.2	0.48	Monotonic	[42]	0.83	0.021	0.025
No	17.5	4	2.4	0.3	1.2	Monotonic	[42]	0.83	0.021	0.013
No	17.5	4	2.4	0.3	1.2	Monotonic	[42]	0.83	0.021	0.017
Yes	17.5	4	2.4	0.3	0.9	Monotonic	[42]	0.83	0.036	0.025
Yes	17.5	4	2.4	0.3	0.9	Monotonic	[42]	0.83	0.036	0.022
No	17.5	4	2.4	0.3	1.2	Monotonic	[42]	0.83	0.027	0.026
No	17.5	4	2.4	0.3	1.2	Monotonic	[42]	0.83	0.027	0.026
No	17.5	4	2.4	0.3	1.2	Monotonic	[42]	0.83	0.021	0.023
No	17.5	2.45	2.3	0.2	0.49	Monotonic	[42]	1.18	0.02	0.023
No	20	4	2.4	0.4	1.6	Monotonic	[43]	0.95	0.024	0.023
No	20	4	2.4	0.2	0.8	Monotonic	[43]	0.95	0.024	0.024
No	20	4	2.4	0.2	0.8	Monotonic	[43]	0.95	0.073	0.044
No	20	4	2.4	0.2	0.8	Monotonic	[43]	0.95	0.067	0.044
No	20	4	2.4	0.2	0.8	Monotonic	[43]	0.95	0.024	0.051
No	20	4	2.4	0.2	0.8	Monotonic	[43]	0.95	0.112	0.075
No	20	4	2.4	0.2	0.8	Monotonic	[43]	0.95	0.024	0.024
No	20	4	2.4	0.4	1.6	Monotonic	[43]	0.95	0.024	0.02
No	20	4	2.4	0.4	1.6	Monotonic	[43]	0.95	0.024	0.02
No	20	4	2.4	0.2	0.8	Monotonic	[43]	0.95	0.032	0.038
No	18.9	1.05	1.37	0.24	0.25	Cyclic	[44]	3.28	0.33	0.212
No	20	3.5	3.07	0.29	1.02	Cyclic	[45]	0.46	0.05	0.057
No	19.0 *	2	1.3	0.2	0.4	Cyclic	[46]	0.99	0.044	0.042
No	20.1	1.2	1	0.31	0.37	Cyclic	[50]	1.06	0.06	0.035
No	20.1	1.2	1	0.31	0.37	Cyclic	[50]	1.06	0.06	0.037
No	20.1	1.2	1	0.31	0.37	Cyclic	[50]	1.06	0.06	0.037
No	19.0 *	1.02	0.9	0.2	0.2	Cyclic	[51]	2.34	0.309	0.152
No	18.1	1	0.9	0.2	0.2	Cyclic	[52]	2.34	0.308	0.161

Table 2. Cont.

Openings	Unit Weight (kN/m ³)	Length (m)	Height (m)	Thickness (m)	Area (m ²)	Cyclic or Monotonic	Reference	f_m (MPa)	σ (MPa)	τ (MPa)
No	19.0 *	1.9	1.2	0.2	0.38	Cyclic	[53]	5.3	0.261	0.117
No	19.0 *	3.06	1.93	0.3	0.92	Cyclic	[54]	0.45	0.026	0.042
No	19.0 *	1.7	1.1	0.24	0.41	Cyclic	[56]	2.37	0.099	0.094
No	19.0 *	1	0.9	0.2	0.2	Cyclic	[9]	2.34	0.309	0.173
No	19.0 *	1	0.9	0.2	0.2	Cyclic	[9]	2.34	0.309	0.217

NA: not available. * The reference does not specify the unit weight of the material, so a value of 19 kN/m³ is assumed for the calculation of the axial stress at the mid-height of the wall. This value is the average of the data collected for unit weight.

Table 3. Compilation of data from tests on RE walls subjected to in-plane shear loads.

Openings	Unit Weight (kN/m ³)	Length (m)	Height (m)	Thickness (m)	Area (m ²)	Cyclic or Monotonic	Reference	f_m (MPa)	σ (MPa)	τ (MPa)
No	18.2	0.5	0.5	0.11	0.06	Monotonic	[8]	0.91	0.105	0.079
No	18.2	0.5	0.5	0.11	0.06	Monotonic	[8]	0.91	0.155	0.095
No	18.2	0.5	0.5	0.11	0.06	Monotonic	[8]	0.91	0.205	0.132
No	18.2	0.5	0.5	0.11	0.06	Monotonic	[8]	0.98	0.105	0.086
No	18.2	0.5	0.5	0.11	0.06	Monotonic	[8]	0.98	0.155	0.115
No	18.2	0.5	0.5	0.11	0.06	Monotonic	[8]	0.98	0.205	0.14
No	19	0.5	0.5	0.11	0.06	Monotonic	[8]	1.31	0.155	0.144
No	19	0.5	0.5	0.11	0.06	Monotonic	[8]	1.31	0.205	0.194
No	19	0.5	0.5	0.11	0.06	Monotonic	[8]	1.65	0.155	0.162
No	19	0.5	0.5	0.11	0.06	Monotonic	[8]	1.65	0.205	0.19
No	18.1	2.4	2.1	0.6	1.44	Cyclic	[10]	3.5	0.024	0.053
No	15	2.4	2.1	0.6	1.44	Cyclic	[10]	1.74	0.021	0.028
No	15.1	2.4	2.1	0.6	1.44	Cyclic	[10]	1.89	0.021	0.016
Yes	19.5	5.66	5.7	0.65	3.03	Cyclic	[11]	1.29	0.108	0.042
Yes	19.5	5.66	2.69	0.65	2.38	Cyclic	[11]	1.29	0.052	0.03
No	19.5	1.2	1.2	0.6	0.72	Monotonic	[19]	1.17	0.012	0.018
No	20	2.5	1.8	0.4	1	Cyclic	[22]	0.54	0.087	0.033
No	20	2.5	1.8	0.4	1	Cyclic	[22]	0.54	0.067	0.03
No	20	2.5	1.8	0.4	1	Cyclic	[22]	0.54	0.038	0.017
No	22.2	1.2	2.5	0.6	0.72	Cyclic	[22]	0.54	0.057	0.022
No	22.2	1.2	1.5	0.6	0.72	Cyclic	[22]	0.54	0.072	0.025
No	22.2	2.1	1.5	0.6	1.26	Cyclic	[22]	0.54	0.05	0.02
Yes	17.8	7	3.45	0.6	2.7	Cyclic	[23]	0.54	0.051	0.025
No	21.1	1.5	1	0.25	0.38	Monotonic	[27]	1.2	0.311	0.096
No	21.1	1.5	1	0.25	0.38	Monotonic	[27]	1.2	0.311	0.139
No	21.1	1.5	1.5	0.25	0.38	Monotonic	[27]	1.2	0.316	0.105
No	21.1	1.5	1.5	0.25	0.38	Monotonic	[27]	1.2	0.316	0.115
No	20	2.8	1.8	0.4	1.12	Cyclic	[34]	0.56	0.029	0.097
No	19.0 *	1.5	1.5	0.25	0.38	Monotonic	[36]	0.97	0.181	0.105
No	19.0 *	1.5	1.5	0.25	0.38	Monotonic	[36]	0.97	0.181	0.115
No	19.0 *	1.5	1	0.25	0.38	Monotonic	[36]	0.97	0.177	0.099
No	19.0 *	1.5	1	0.25	0.38	Monotonic	[36]	0.97	0.177	0.139
No	21	1.9	1.2	0.25	0.48	Cyclic	[38]	0.96	0.213	0.234
No	21	1.9	0.45	0.35	0.67	Cyclic	[39]	NA	0.205	0.105
No	21	1.9	0.45	0.35	0.67	Cyclic	[39]	NA	0.205	0.093
No	19.0 *	1.05	1.3	0.25	0.26	Cyclic	[40]	3.73	0.572	0.281
No	19.0 *	1.05	1.3	0.25	0.26	Cyclic	[40]	3.73	0.572	0.227
No	19.0 *	1.05	1.3	0.25	0.26	Cyclic	[40]	3.73	0.572	0.292
No	19.0 *	1.5	1.5	0.2	0.3	Cyclic	[47]	1.47	0.014	0.178
No	19.4	1	0.9	0.2	0.2	Cyclic	[48]	1.17	0.109	0.145
No	19.4	1	0.9	0.2	0.2	Cyclic	[48]	1.17	0.209	0.167
No	19.4	1	0.9	0.2	0.2	Cyclic	[48]	1.17	0.309	0.21

Table 3. Cont.

Openings	Unit Weight (kN/m ³)	Length (m)	Height (m)	Thickness (m)	Area (m ²)	Cyclic or Monotonic	Reference	f'_m (MPa)	σ (MPa)	τ (MPa)
No	20	2.4	2.1	0.6	1.44	Monotonic	[49]	1.36	0.081	0.051
No	17.8	1.25	1.25	0.25	0.31	Cyclic	[55]	2.28	0.201	0.06
No	17.8	1.25	1.25	0.25	0.31	Cyclic	[55]	2.28	0.201	0.063
No	17.8	1.25	1.25	0.25	0.31	Cyclic	[55]	2.19	0.201	0.06
No	17.8	1.25	1.25	0.25	0.31	Cyclic	[55]	2.19	0.201	0.057
No	17	1.5	1.5	0.25	0.38	Monotonic	[58]	1.15	0.335	0.107
No	17	1.5	1.5	0.25	0.38	Monotonic	[58]	1.15	0.335	0.115
No	17	1.5	1	0.25	0.38	Monotonic	[58]	1.15	0.33	0.096
No	17	1.5	1	0.25	0.38	Monotonic	[58]	1.15	0.33	0.139

* The reference does not specify the unit weight of the material, so a value of 19 kN/m³ is assumed for the calculation of the axial stress at the mid-height of the wall. This value is the average of the data collected for unit weight.

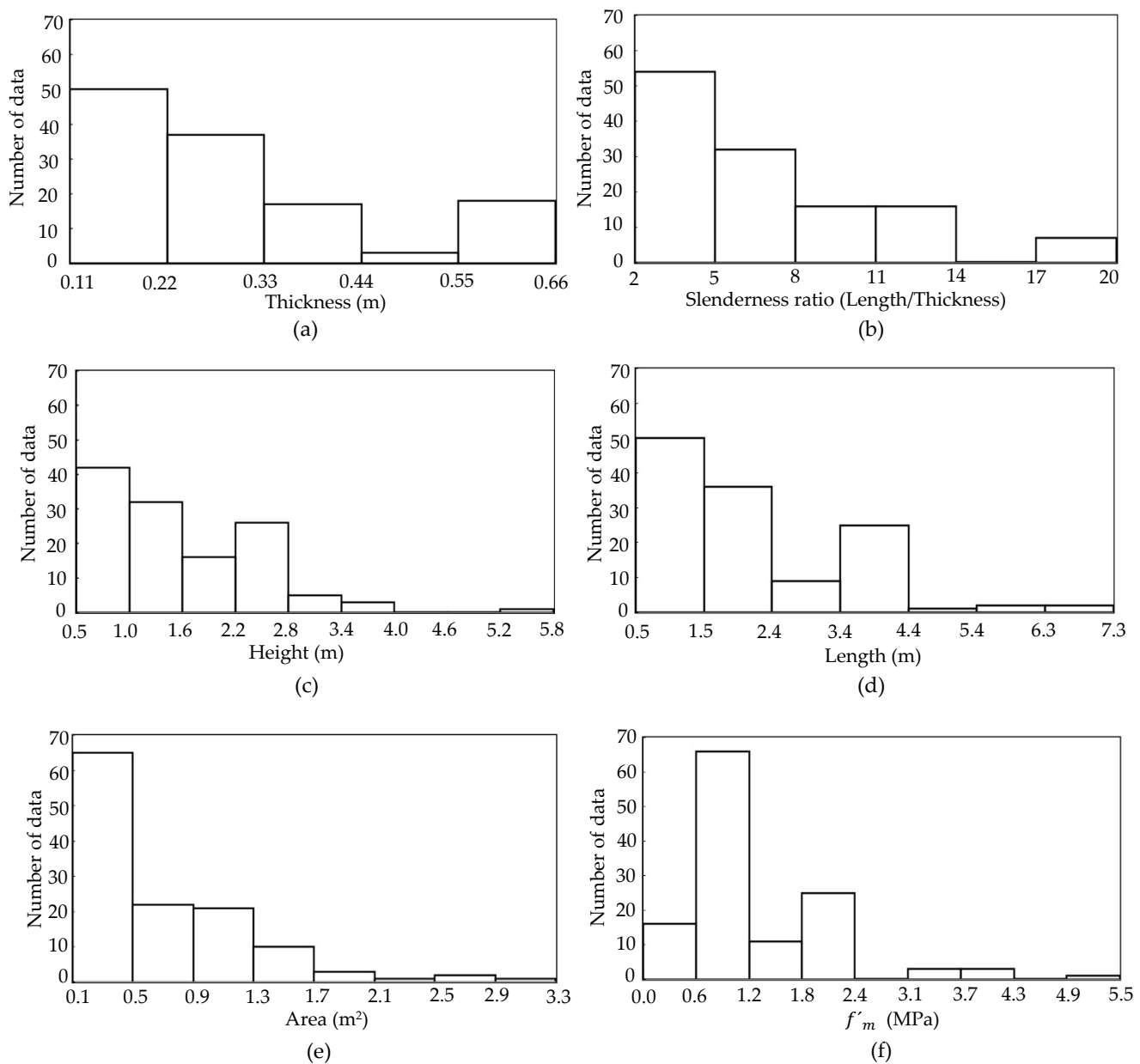


Figure 3. Histogram of frequencies of geometric variables: (a) thickness; (b) slenderness; (c) height; (d) length; (e) area; (f) f'_m .

A critical variable for determining the average shear strength of the tested walls is the cross-sectional area, calculated as the product of length and thickness for walls without openings. Statistical analyses reveal that approximately 60% of the tests documented in the collected literature correspond to walls with cross-sectional areas smaller than 0.5 m^2 , as shown in Figure 3e. Regarding mechanical properties, Figure 3f illustrates the frequency histogram of compressive strength (f'_m) for both adobe and RE. The compressive strength values predominantly fall below 2.4 MPa, consistent with the findings of [59], who reported compressive strength values below 2.55 MPa for unstabilized RE. Furthermore, Ref. [59] documented a mean compressive strength of 1.55 MPa, closely aligning with the statistical mean of 1.44 MPa calculated from the current dataset. For unstabilized adobe masonry, Ref. [60] reported an average compressive strength of approximately 1.3 MPa, which is similar to the values observed for unstabilized RE in this study.

Figure 4 presents a detailed examination of the relationship between axial stress (σ) and shear strength (τ) for adobe walls (Figure 4a), RE walls (Figure 4b), and the combined dataset (Figure 4c). In Figure 4a, the data for adobe walls show a strong correlation between axial and shear strength ($R^2 = 0.8195$), highlighting a cohesive–frictional behavior characteristic of this material. While the trend line provides a good representation of the dataset, the dispersion of points indicates the variability in material properties, testing conditions, and construction techniques. In Figure 4b, the behavior of RE walls is analyzed, indicating a slightly weaker correlation ($R^2 = 0.5281$) compared to adobe. The trend lines reveal that RE walls generally exhibit higher shear strength than adobe walls under comparable axial stresses, likely due to their denser composition and enhanced interlayer bonding. The greater variability observed in the RE dataset may reflect differences in granulometry, compaction quality, and material heterogeneity. Data points from Colombian tests, marked in red, are consistently located near the lower range of values, emphasizing the importance of full-scale experiments in capturing realistic material performance. Figure 4c, which integrates data from both materials, illustrates the cohesive–frictional behavior characteristic of earthen walls, with a regression equation yielding an R^2 value of 0.7068. The inclusion of a 99% confidence interval underscores the inherent variability of these materials, which is influenced by differences in composition, testing protocols, and construction practices.

The AIS-610-EP-2017 standard [61] (Evaluation and Intervention of One- and Two-Story Adobe and RE Heritage Buildings) includes a Mohr–Coulomb failure curve that is incorporated into all plots in Figure 4, serving as a conservative baseline for the design of earthen walls. This curve closely aligns with the lower bound of the dataset, providing safe and reliable estimations of shear strength for adobe and RE walls under varying axial stress conditions. Such conservatism is essential in seismic regions, where variability in material properties and construction practices can significantly impact structural performance. These findings validate the relevance and applicability of the AIS-610-EP-2017 curve, emphasizing the importance of integrating data from full-scale experimental tests to refine its accuracy and ensure its continued effectiveness in guiding safe design practices.

Plotting shear strength against cross-sectional area resulted in the relationships illustrated in Figure 5. Shear strength was calculated by dividing the resisting shear force by the cross-sectional area at the mid-height of the tested wall. The data presented in Figure 5a,b demonstrate a pronounced inverse relationship between wall area and shear strength for both adobe and RE specimens. Independent of the axial load stress, as the wall area decreases, the measured shear strength consistently increases, reflecting a notable scale effect. This behavior underscores the tendency of smaller specimens to display higher apparent shear strength, likely due to a reduced likelihood of encountering material heterogeneities and the influence of simplified stress distributions during testing.

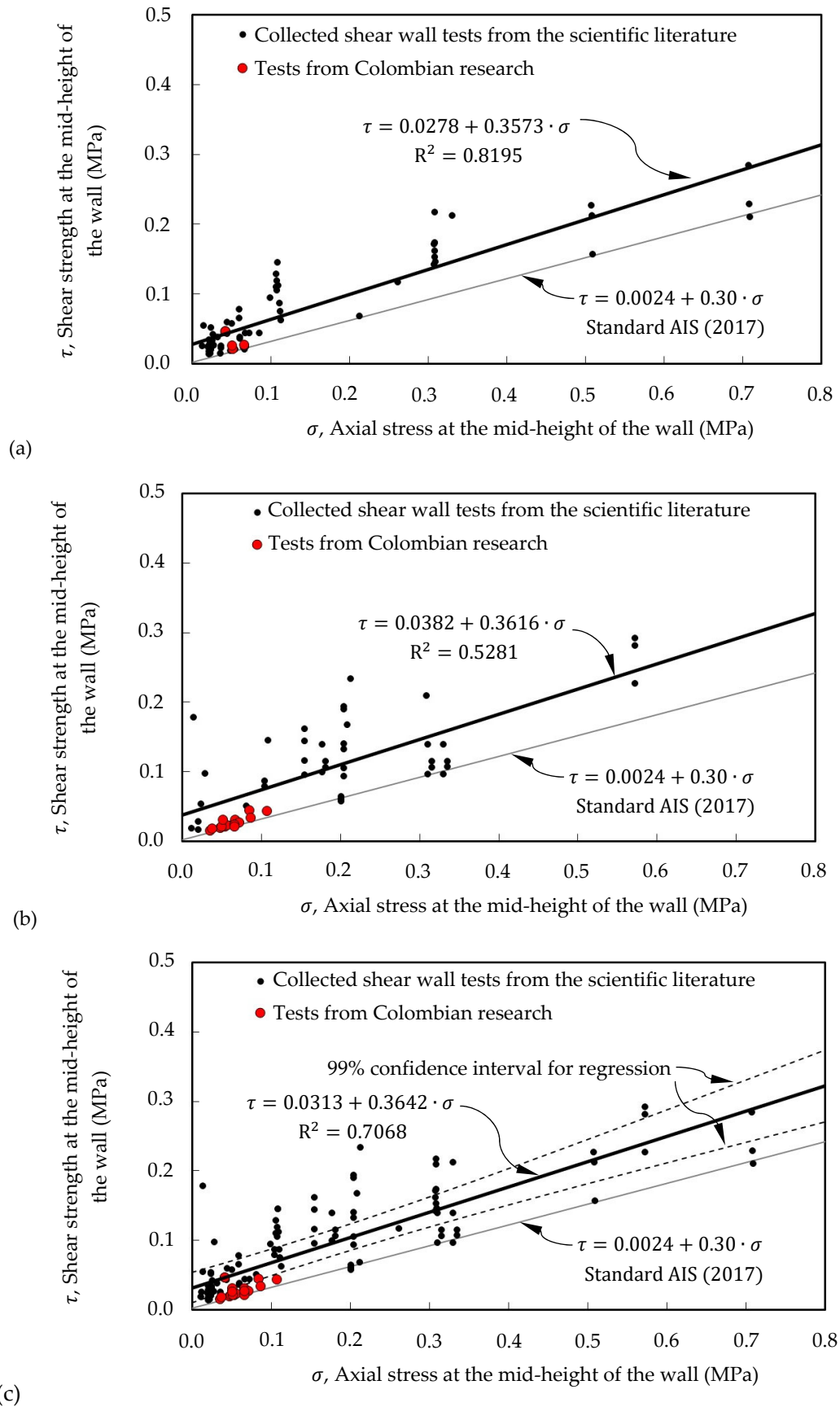


Figure 4. Axial stress vs. shear stress according to the collected data from in-plane shear tests of earthen walls (adobe and RE): (a) adobe; (b) RE; (c) both adobe and RE. The mentioned reference is AIS (2017) [61].

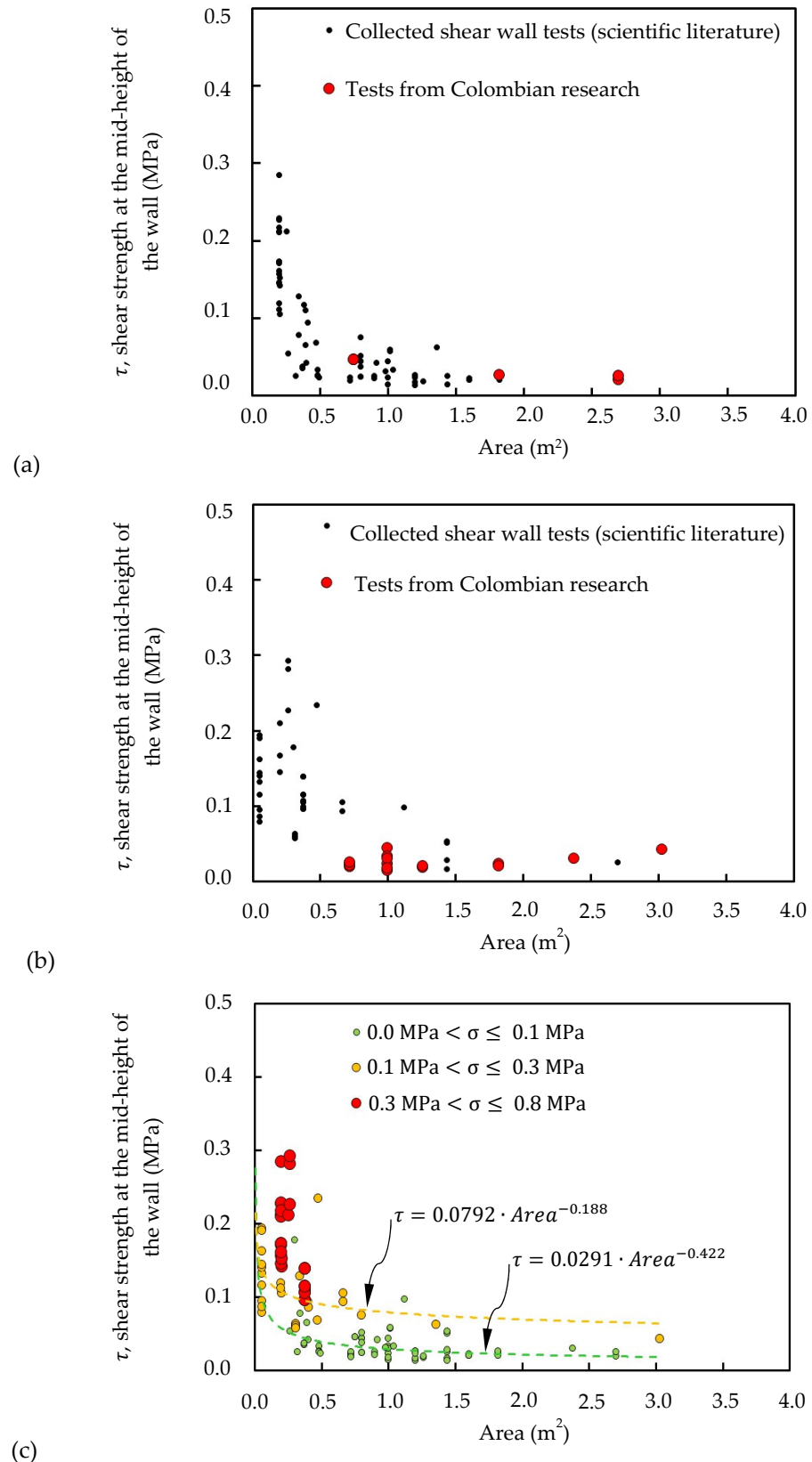


Figure 5. Shear strength vs. area of the tested walls according to the collected data of shear in-plane tests of earthen walls (adobe and RE): (a) adobe; (b) RE; (c) both adobe and RE with different axial stresses.

When both materials are analyzed together, as shown in Figure 5c, the general trend remains consistent: smaller-scale tests systematically overestimate the shear strength of

earthen walls. These findings have critical implications for the development of building codes and design guidelines, highlighting the importance of accounting for scale effects when interpreting laboratory results and extrapolating them to real-world applications.

In Figure 5c, axial stress is introduced as an additional variable, represented by markers in three distinct colors: green for low axial stress ($0.0 \text{ MPa} < \sigma \leq 0.1 \text{ MPa}$), yellow for intermediate axial stress levels ($0.1 \text{ MPa} < \sigma \leq 0.3 \text{ MPa}$), and red for high axial stress ($0.3 \text{ MPa} < \sigma \leq 0.8 \text{ MPa}$). The results clearly demonstrate the significant influence of axial stress on shear strength, comparable in importance to the size of the tested specimens. The statistical data in Figure 5c indicate a broader range of specimen sizes (areas) tested under medium and low axial stresses, whereas fewer tests involve full-scale specimens under high axial stresses. This trend is likely due to the uncommon presence of multi-story earthen buildings in seismic zones, as such structures typically have fewer than three stories [62]. These types of constructions typically exhibit maximum axial stresses below 0.3 MPa at the mid-height of critical walls. Consequently, the subsequent analysis focuses exclusively on axial force ranges below 0.3 MPa.

For medium and low axial stress ranges, the recommended specimen size (area) for evaluating shear strength through the in-plane shear testing of walls was determined. This process involved analyzing the relationship between shear resistance (τ) and wall area using regression equations derived from experimental data. For each axial stress range, a regression model of the form $\tau = a \cdot (\text{Area})^b$ was applied, where the constants a and b were determined based on the experimental results. These equations captured how shear resistance decreases as wall area increases, demonstrating the scale effect commonly observed in earthen walls. Figure 5c and Table 4 present the regression models and their equations for the cases analyzed. To establish the minimum wall area where shear strength estimates become stable (i.e., where the slope of the relationship between shear strength and wall area approaches zero), the derivative of the regression equation ($\frac{d\tau}{d\text{Area}}$) was calculated for each axial stress range. A steady-state condition was defined as $\left(\frac{d\tau}{d\text{Area}}\right) < 0.03$ (proposed by the authors), indicating that the rate of change in shear strength with respect to wall area is negligible (less than 3%), essentially when the curve flattens out. Solving this inequality provided the critical wall area for each axial stress range. The results, summarized in Table 4, show that the critical wall area is similar across the ranges analyzed, with a recommended area $\geq 0.5 \text{ m}^2$. This corresponds, for example, to wall dimensions of $1.7 \text{ m} \times 2.0 \text{ m} \times 0.3 \text{ m}$ (length \times height \times thickness). These findings highlight the importance of using appropriately sized wall specimens in laboratory shear tests to ensure results that accurately represent real-world full-scale structural behavior.

Table 4. Minimum wall areas for accurate shear strength estimation in laboratory tests.

Range of Axial Stress	Regression Between Shear Strength (τ) and Area (A)	$\left \frac{d\tau}{d\text{Area}}\right < 0.03$
$0.0 \text{ MPa} < \sigma \leq 0.1 \text{ MPa}$	$\tau = 0.0291 \cdot A^{-0.422}$	$\left 0.0291 \cdot 0.422 \cdot \text{Area}^{-1.422}\right < 0.03 \mid \text{Area} > 0.53 \text{ m}^2$
$0.0 \text{ MPa} < \sigma \leq 0.3 \text{ MPa}$	$\tau = 0.0792 \cdot A^{-0.188}$	$\left 0.0792 \cdot 0.188 \cdot A^{-1.188}\right < 0.03 \mid \text{Area} > 0.55 \text{ m}^2$

3.2. Collected Database: Direct Shear Tests from the Literature

Recent research has extensively examined the mechanical properties of RE and adobe, with a specific focus on their shear strength parameters cohesion (c) and friction angle (ϕ). These parameters have traditionally been used to understand the structural behavior of earthen materials, although many complex and comprehensive models are currently avail-

able for modeling soil behavior. The reviewed research highlights the critical interactions among experimental methodologies, numerical modeling, and environmental factors in determining shear strength. Notably, most of the direct shear test data available in the technical and scientific literature pertain to RE, with such tests being uncommon for adobe. Among the references consulted, and as summarized in Table 5, only one direct shear test on unstabilized adobe was identified. This limited dataset underscores the need for more experimental studies focused on adobe. Furthermore, the variability in cohesion and friction angle reported in Table 5 reflects the influence of material composition, testing scale, and other inherent factors in unstabilized earthen materials.

Table 5. Strength parameters (cohesion c , and friction angle ϕ) for RE and adobe reported in the consulted references.

Model ID	Reference	ϕ (°)	c (MPa)	Dimensions of the Specimen Tested or Numerical Model	Comments
1	[63]	37	0.5600	Model	
2	[6]	45	0.1300	Model	
3	[64]	37	0.1890	Model	
4	[65]	51	0.1700	40 × 40 × 65 mm	Model and experimental research
5	[66]	41	0.0134	Diameter = 76.2 mm height = 147.2 mm	Cylindrical specimen
6	[21]	37	0.0309	490 × 490 × 450 mm	Big and intralayer specimen
7	[21]	35	0.0240	490 × 490 × 450 mm	Big and intralayer specimen
8	[58]	35	0.0303	490 × 490 × 360 mm	Big and layer specimen
9	[58]	33	0.0247	490 × 490 × 360 mm	Big and interface specimen
10	[58]	44	0.2630	100 × 100 × 40 mm	Small and upper layer specimen
11	[58]	46	0.1350	100 × 100 × 40 mm	Small and middle layer specimen
12	[7]	44	0.1640	100 × 100 × 35 mm	Middle part of the layer specimen
13	[7]	44	0.2635	100 × 100 × 35 mm	Upper part of the layer specimen
14	[13]	65	0.0500	150 × 150 × 189 mm	
15	[20]	37	0.5610	Model	
16	[67]	51	0.3084	Diameter = 62 mm height = 25 mm	Moisture = 4.2%
17	[67]	41	0.3000	Diameter = 62 mm height = 25 mm	Moisture = 6.0%
18	[61]	17	0.0024		Colombian standard
19	[68]	41	0.0151	270 × 150 × 150 mm	Adobe and joint mud mortar
N/A	[69]	*	0.0301	310 × 150 × 320 mm	Molded adobe and mud mortar
N/A	[69]	*	0.0102	370 × 240 × 200 mm	Rammed adobe and mud mortar
N/A	[69]	*	0.0273	240 × 115 × 179 mm	Extruded earth block and mud mortar

* Shear strength tests with no axial load applied. N/A: not applicable.

The authors of [63] provided insights through experimental testing and finite element modeling, reporting a friction angle of 37° and a cohesion value of 0.560 MPa. This work highlights the importance of accounting for nonlinear stress–strain relationships in RE walls, emphasizing their inherent material variability. The authors of [6] advanced the field by using discrete element modeling to simulate the failure of RE walls under lateral loads. Their findings included a friction angle of 45° and a cohesion of 0.130 MPa, demonstrating that numerical approaches could complement experimental methods to capture the complexities of soil–structure interactions. The authors of [65] explored combined modeling and experimental techniques, identifying higher values for the friction angle (51°) and moderate cohesion (0.170 MPa) in similar materials, further supporting the applicability of discrete models for structural predictions. The authors of [20,64] contributed to the understanding of RE's shear behavior and reported values of $\phi = 37^\circ$ and $c = 0.189$ MPa, aligned

closely with the findings of [63]. The authors of [20] also presented cohesion values as high as 0.561 MPa, reflecting the influence of specimen preparation and test setup. Another study [66] employed finite element modeling to analyze the elastoplastic behavior of RE walls; this study reported a friction angle of 41° and a low cohesion value of 0.0134 MPa, underscoring the impact of water content on material strength. These results highlight the role of environmental conditions in determining the performance of earthen materials.

A significant contribution came from El-Nabouch and colleagues [7,21,29,58], who extensively studied the shear parameters of RE through a series of experiments (direct shear tests) and numerical validations. The authors of [7,21] used large shear boxes ($490 \times 490 \times 450$ mm) and direct shear boxes of smaller sizes ($100 \times 100 \times 40$ mm) to investigate the interface, interlayer, and intralayer (upper layer and middle part of the layers) behavior of RE materials, reporting ϕ values ranging from 35° to 44° and cohesion values between 0.024 MPa and 0.264 MPa. Their findings demonstrated significant variations in shear parameters, influenced by both layer position and the scale of testing. Specifically, intralayer tests exhibited higher cohesion values compared to interlayer tests, highlighting the critical role of layer interfaces in maintaining structural integrity. The authors of [13] reported an exceptionally high friction angle of 65° and a cohesion value of 0.05 MPa. Complementarily, Ref. [67] examined the influence of moisture on adobe's shear strength, finding friction angles of 51° at 4.2% moisture and 41° at 6% moisture content, although their reported cohesion values were similar. The authors of [69] performed shear strength tests on earthen bricks bonded with mud mortar, explicitly excluding the application of axial load. Consequently, the findings emphasized material cohesion, with no friction angle values reported. The tests produced average cohesion values ranging from 0.01 MPa to 0.03 MPa. Finally, the standard [61] provides baseline values for traditional earthen constructions (the same parameters for adobe and RE) and is also the lower bound of the data collected for adobe and RE walls subjected to pseudo-static in-plane load tests, with $\phi = 17^\circ$ and $c = 0.0024$ MPa. These conservative parameters serve as benchmarks for assessing the safety and feasibility of heritage structures built with unstabilized materials.

Unlike geotechnical characterization, direct shear tests on large specimens of RE or adobe are essential to capture mechanical behaviors associated with compaction layers, material heterogeneity, interactions between compaction layers, and mortar–adobe brick interfaces. These critical variables cannot be effectively observed in small specimens. Consequently, the authors of the referenced studies conducted direct shear tests on specimens with rectangular cross sections (e.g., parallelepipeds) or, alternatively, on cylindrical specimens. Additionally, some studies have relied on numerical modeling to complement their experimental findings. Table 5 summarizes the dimensions of the specimens tested using the direct shear test protocol. Specifically, Refs. [6,20,63,64] employed numerical models to simulate materials' behavior. Conversely, Ref. [65] used small specimens with dimensions of $40 \times 40 \times 65$ mm, which may limit the ability to capture large heterogeneities. The authors of [66] used cylindrical specimens with a diameter of 76.2 mm and a height of 147.2 mm, in line with typical geotechnical testing standards, while [21,58] consistently used large specimens measuring $490 \times 490 \times 450$ mm for intralayer and interlayer shear tests, providing more representative results of the actual performance of RE materials. In addition, smaller specimens measuring $100 \times 100 \times 40$ mm and $100 \times 100 \times 35$ mm were used by [7] for comparison purposes. The authors of [13] used specimens measuring $150 \times 150 \times 189$ mm, reflecting a balance between capturing representative behavior and practical constraints. The studies reported in [67] followed the ASTM standards, using cylindrical specimens with a diameter of 62 mm and different heights (25 mm and 35 mm).

4. Direct Cyclic Shear Tests Performed on RE Material (300 × 300 × 300 mm Specimens)

The authors of [11] presented the largest full-scale two-story rammed-earth (RE) wall ever tested globally under pseudo-static loading conditions. This wall was constructed and tested at the Structures Laboratory of the Pontificia Universidad Javeriana in a research collaboration with Universidad de los Andes, Colombia. Figure 6 illustrates the RE wall (Figure 6a) along with the experimental setup (Figure 6b). The experimental setup used by the authors of [11] consisted of two servo-controlled hydraulic actuators applying in-plane cyclic shear loads to the first and second floors of the tested wall. A 250 kN actuator was positioned at the second level, while a 100 kN actuator was installed at the first level to ensure controlled load application. To monitor the wall's response, 14 LVDTs were placed at various heights to record the displacement profiles during both push and pull cycles. Additionally, a distributed load of 5.3 kN/m was applied to simulate the weight of a conventional earthen construction roof. To further enhance the displacement measurement accuracy, LIDAR (Light Detection and Ranging) technology was used, employing 3D laser scanning to track the movement of over 150 million points on the wall's surface. This provided high-resolution spatial data, enabling detailed validation of the displacement profiles and deformation behavior throughout the test. The experiment was conducted under simultaneous displacement control at both levels, with a predefined ratio of 2.0 between second-floor and first-floor displacement, programmed through the MTS control system [11].

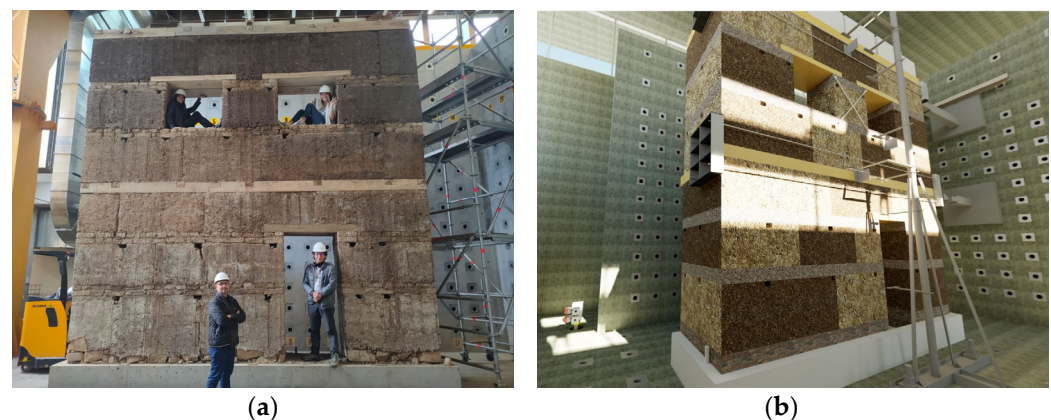


Figure 6. (a) Two-story RE wall; (b) experimental setup for pseudo-static test.

To validate the preliminary conclusions from Section 3, specimens for cyclic direct shear tests were prepared using identical materials, craftsmanship, and construction methods as those employed in the full-scale two-story wall (Figure 6a). Large cubic specimens (300 mm per side) were fabricated for cyclic shear testing, alongside uniaxial compression specimens, as shown in Figure 7. All specimens underwent a 40-day drying period. Consistent with the full-scale two-story RE wall (5.95 m in length, 6.20 m in height, and 0.65 m in thickness), the specimens for the shear and compression tests were constructed using compaction layers of approximately 7.5 to 10 cm in thickness.

The experimental setup for the cyclic direct shear tests used two high-precision MTS actuators: one vertical actuator to precisely apply the axial load, and another horizontal actuator, with a maximum capacity of 100 kN and a stroke of ± 125 mm, to apply the horizontal displacement protocol (Figure 8a,b). The instrumentation included two load cells (one per actuator), the internal LVDTs of the actuators, and two MTS laser deformimeters to measure the displacements and shear strains on each tested specimen. These laser sensors monitored the shear displacements on two lateral (parallel) faces of the cubic specimens

(300 mm per side). The experimental setup was specifically designed by the researchers to minimize friction and ensure accurate axial load control while applying displacement-controlled forces. To achieve this, the RE cubes were placed on a steel plate supported by spheres, as shown in Figure 8c,d. The cyclic loading protocol followed the guidelines outlined in [70] and is presented in Figure 9a. Horizontal displacements were applied at a frequency of 0.1 Hz, with the actuator maintaining uniform cyclic loads until failure or a strain level of 10%. Compressive strength was evaluated after one month of drying following the compaction of the specimens (a total of 10 specimens of $500 \times 500 \times 250$ mm were tested in compression). The average compressive strength was 1.29 MPa, with a coefficient of variation of 17%. Proctor tests according to standard [71] were also performed, with an average maximum dry density of 16.49 kN/m^3 and an optimal moisture content of 16.48%. For the direct cyclic shear test, three axial stress values were selected to cover the typical range of vertical working stresses in earthen buildings of 1 to 3 stories. This corresponds to maximum vertical stresses of approximately 0.2 MPa. The chosen stress values were 184, 79, and 24 kPa, respectively.



Figure 7. (a) RE specimens with dimensions of $300 \times 300 \times 300$ mm for direct cyclic shear test; (b) compression and shear specimens during drying process.

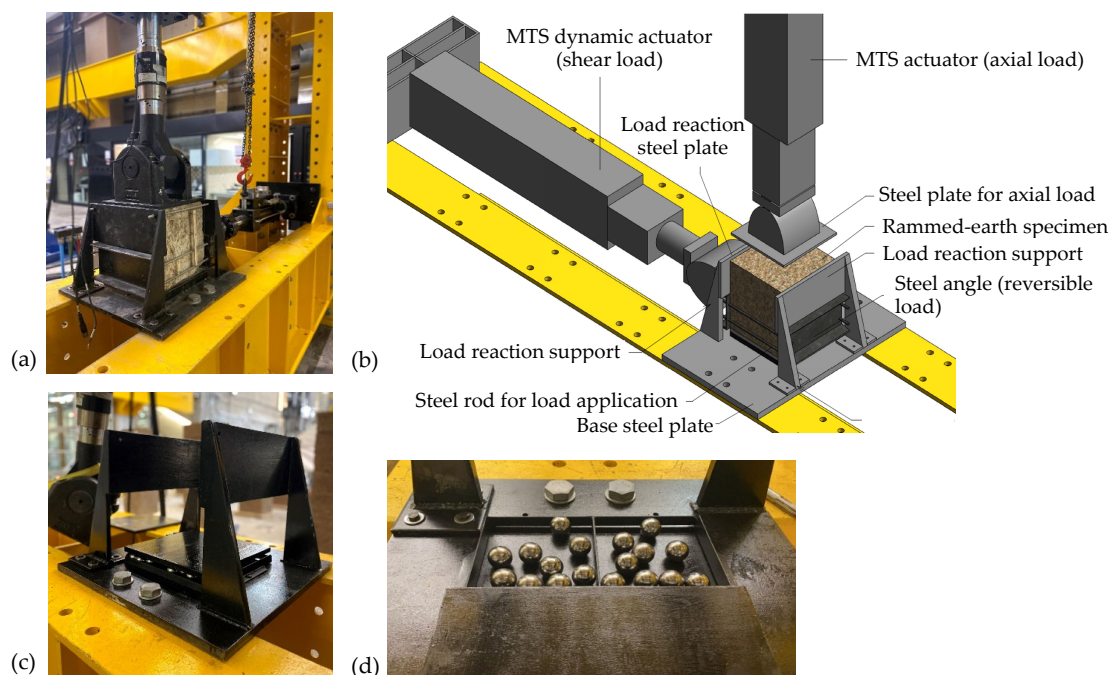


Figure 8. (a) Photograph of the setup for the direct cyclic shear test performed on RE specimens; (b) components of the test setup; (c,d) spheres to support the cubic specimens in order to minimize friction in the test setup.

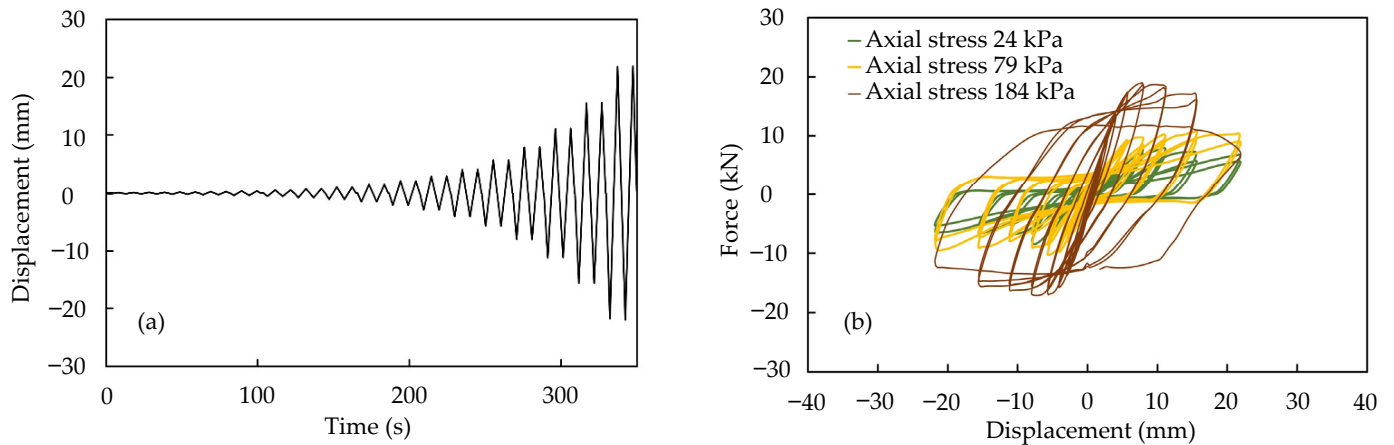


Figure 9. (a) Horizontal load protocol (displacement controlled); (b) hysteresis loops for the three axial stresses considered.

Figure 9b presents the hysteresis curves from the direct cyclic shear tests at the three axial stress levels. According to the results, the shear resistance and energy dissipation increase with axial stress. At 24 kPa, the curve shows narrow loops with low force magnitudes, indicating minimal energy dissipation and reduced shear resistance due to limited confinement. As the axial stress increases to 79 kPa, the hysteresis curve shows wider loops and higher force magnitudes, reflecting improved shear resistance and greater energy dissipation. At 184 kPa, the curve shows the widest loops and highest forces, highlighting the role of enhanced confinement in maximizing shear strength and energy dissipation. For all conditions, the displacement range remains constant, but the force magnitudes increase significantly with axial stress. The curves also show nonlinear behavior and slight stiffness degradation, especially at lower axial stresses, as the loops shift to larger displacements with repeated loading.

Figure 10 presents the final state of the nine specimens tested under axial stresses of 184, 79, and 24 kPa. The photographs reveal that shear failure predominantly occurs along compaction layers or intermediate zones, which act as inherent planes of weakness within the material. At 184 kPa, the highest axial stress, the failure surfaces are well defined and localized, indicating enhanced shear resistance due to increased confinement. At 79 kPa, the shear planes are less continuous, with cracking mechanisms distributed across the specimens. At 24 kPa, the lowest axial stress, failure becomes more diffuse and irregular, with extensive cracking, reflecting reduced shear resistance and brittle behavior under minimal confinement. These failure patterns highlight the influence of axial stress on shear response: higher stress promotes localized failure and improved strength, while lower stress results in a broader damage spread.

Figure 11a illustrates the Mohr–Coulomb failure envelope derived from the cyclic direct shear test results (green triangles), contrasted with the full-scale two-story RE wall reported in [11,23] (green diamonds). The authors of [23] detailed the testing of a one-story RE wall measuring 7.0 m in length, 3.45 m in height, and 0.6 m in thickness, featuring door and window openings. The authors of [11], on the other hand, reported the testing of a two-story RE wall, measuring 5.95 m in length, 6.20 m in height, and 0.65 m in thickness. Both the two-story rammed earth wall tested with in-plane shear loading and the 300 mm side cubes tested with the cyclic direct shear protocol were constructed using the same materials and construction methods. The linear trend line from the present study (cyclic shear tests, Figure 11a, green triangles) indicates an apparent cohesion of 0.0715 MPa and a slope of 0.6608, corresponding to a friction angle of 33.5° . The high R^2 value of 0.9828 demonstrates a strong correlation between axial stress and shear stress, validating the applicability of

the Mohr–Coulomb failure criterion to describe the material’s behavior. Also, these values reflect a moderate shear resistance, typical of cohesive–frictional materials like compacted RE, where both internal friction and cohesion contribute significantly to resisting shear failure. However, a clear discrepancy is observed when comparing these results with the shear strength data from [11,23] (Figure 11a, green diamonds). Specifically, the shear stress values reported for the full-scale wall tests are consistently lower than those obtained in the smaller-scale direct shear tests at similar axial stress levels (apparent cohesion of 0.0139 MPa and a slope of 0.26). When comparing the shear strength data of these full-scale RE walls with the respective strengths estimated from cyclic direct shear tests at the same axial load level, a ratio between 3.4 and 3.8 is observed. This ratio highlights the consistent overestimation of shear strength by small-scale direct shear tests when compared to the structural behavior of real-world walls (full-scale). This difference can be attributed to scale effects and the inherent complexities associated with full-scale structures, e.g., the interactions between massive blocks of RE, interactions between compaction layers, irregular stress distributions, etc.

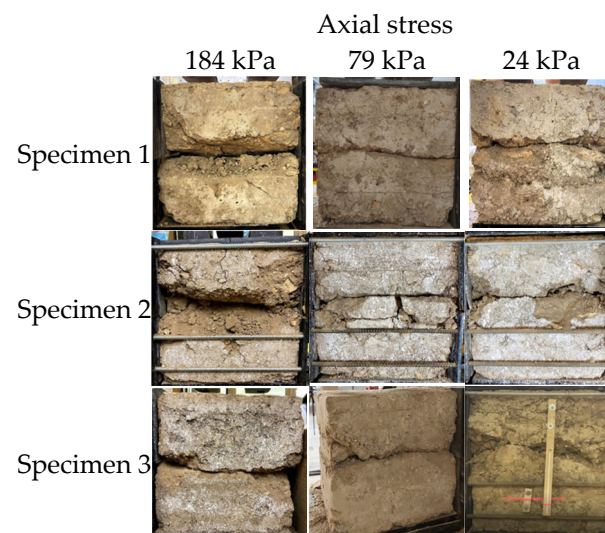


Figure 10. Final state of specimens subjected to cyclic direct shear tests under different axial stress levels.

Similarly, for adobe walls, Figure 11b illustrates the results from full-scale and small-scale direct shear tests. The authors of [23] described the testing of a full-scale adobe wall measuring 7.0 m in length, 3.45 m in height, and 0.6 m in thickness, also featuring door and window openings. Using the same material and construction techniques, nine small adobe masonry specimens were prepared, each consisting of two adobe bricks and a single mud joint (dimensions: 0.27 m long, 0.15 m wide, and 0.15 m high). The joint mortar thickness ranged between 18 mm and 20 mm. The mortar, composed solely of earth and water, exhibited the following physical properties: liquid limit between 34 and 37%, plastic limit of 19%, and a plasticity index ranging from 16% to 18%. Particle size distribution analysis indicated that more than 84% of the material passed sieve #50, while over 68% passed sieve #200. Based on the Unified Soil Classification System (USCS), the mortar soil was classified as lean clay (CL). Additionally, compressive strength tests were conducted on adobe masonry prisms, resulting in an average compressive strength of 1.1 MPa. The shear specimens were subjected to static direct shear tests, as reported in [68]. The results from the small-scale direct shear tests are represented by red triangles in Figure 11b, while the full-scale wall test is represented by a red diamond in Figure 11b. A ratio of approximately 3.0 is observed when comparing the shear strength of the full-scale adobe wall with the corresponding values estimated from static direct shear tests at the same axial load level.

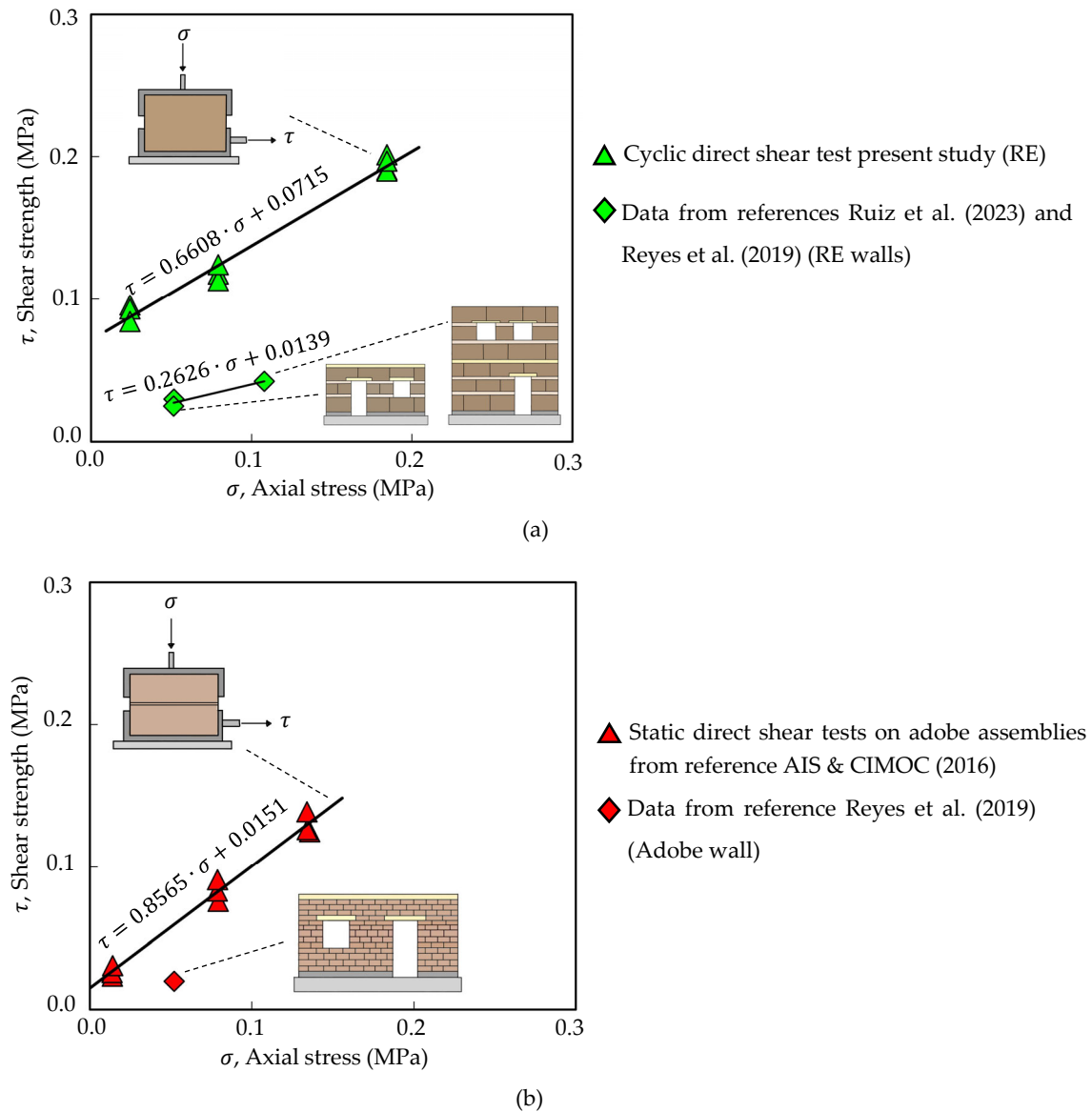


Figure 11. Comparative analysis of Mohr–Coulomb failure envelopes derived from direct shear tests (triangles) and shear strength values obtained from full-scale wall tests (diamonds): (a) rammed earth (RE), the mentioned references are Ruiz et al. (2023) [11] and Reyes et al. (2019) [23]; (b) adobe, the mentioned references are AIS & CIMOC (2016) [68] and Reyes et al. (2019) [23].

These comparisons, shown in Figure 11a for RE walls and Figure 11b for adobe walls, reinforce the need for appropriate scaling adjustments when using small-scale direct shear tests to estimate the structural behavior of full-scale earthen walls. In addition, the results emphasize the critical importance of full-scale testing to capture realistic macro-structural failure mechanisms. Given the importance of these findings, Figure 11 presents detailed visual illustrations, including diagrams of the full-scale wall setups and the direct shear test configurations for small specimens. This approach enhances clarity and facilitates a deeper understanding of the experimental methodologies and their implications.

Similar to the present study [58], conducted both static direct shear tests and in-plane shear tests on wall specimens, applying axial stresses ranging from 0.05 MPa to just below 0.4 MPa. The larger direct shear specimens measured $490 \times 490 \times 360$ mm, while the smaller specimens were $100 \times 100 \times 40$ mm. Additionally, within the same study, and using the same rammed-earth materials, in-plane shear tests were performed on 1.5×1.5 m walls with a thickness of 0.25 m, subjected to vertical loads inducing axial stresses of 0.3 MPa [29].

It is important to note that while the walls tested in [29,58] measured 1.5 m per side and do not fully represent full-scale earthen walls, they still offer a valuable basis for comparison with the findings of this study. According to the results reported in [29], the average maximum shear strength of walls subjected to in-plane shear loading was 0.107 MPa (at an axial stress of 0.3 MPa). In contrast, the shear strength values estimated from small direct shear specimens under the same 0.3 MPa axial stress ranged from 0.44 to 0.55 MPa [58], significantly exceeding the shear strength of the walls. Furthermore, when using large direct shear specimens under the same 0.3 MPa axial stress, the estimated shear strength reported in [58] ranged between 0.22 and 0.24 MPa—still overestimating the wall strength, but substantially lower than the values obtained from small specimens. Table 6 summarizes this analysis, demonstrating that a reduction factor of 3.18 is necessary to adjust small-scale direct shear test results to better represent full-scale wall behavior. This factor closely aligns with the range of 3.0 to 3.8 determined in the present study, further reinforcing the validity of the findings.

Table 6. Comparison between direct shear strengths and in-plane wall shear strengths reported in [29,58].

References	σ (MPa)	τ (MPa)	Type of Tests	Dimensions of the Specimen Tested	Average τ (MPa)	Ratio Between Shear Strength of Small Specimens and Walls
[58]	0.3	0.2194	Direct shear	490 × 490 × 360 mm	0.3647	3.18
[58]	0.3	0.2430	Direct shear	490 × 490 × 360 mm		
[58]	0.3	0.4418	Direct shear	100 × 100 × 40 mm		
[58]	0.3	0.5545	Direct shear	100 × 100 × 40 mm		
[29,58]	0.3	0.0969	In-plane shear	1000 × 1500 × 250 mm	0.1145	
[29,58]	0.3	0.1149	In-plane shear	1500 × 1500 × 250 mm		
[29,58]	0.3	0.1059	In-plane shear	1500 × 1500 × 250 mm		
[29,58]	0.3	0.1403	In-plane shear	1000 × 1500 × 250 mm		

5. Comparative Analysis of Direct Shear Test Results and Shear Strength of Earthen Walls

For comparative purposes, and to extend the observations made in the previous chapter to the information compiled in technical–scientific publications, Figure 12 presents a comprehensive analysis of shear strength results for earthen materials, incorporating data from the present study’s cyclic direct shear tests (green triangles), 125 shear wall tests compiled from the literature and summarized in Tables 2 and 3 (blue circles), and the Mohr–Coulomb failure envelopes reported in prior studies and listed in Table 5 (solid lines). A clear trend emerges from the wall test results: shear strength increases with higher axial stress, consistent with the Mohr–Coulomb failure criterion. However, despite this trend, significant data scatter is observed, reinforcing the complexity of shear resistance in full-scale walls. The figure also demonstrates that failure envelopes derived from direct shear tests overestimate the shear strength of full-scale adobe and RE walls, a discrepancy that becomes apparent when these curves are compared to the conservative failure line of [61] (Colombian standard). While direct shear tests are effective in determining key material parameters such as cohesion and friction angle in soils, they do not account for critical structural factors that influence the shear resistance of full-scale walls under realistic structural conditions (full-scale or near-full-scale). These factors include density variations, pores, voids in the material, and the presence of openings such as doors and windows, which significantly reduce the mechanical performance of a wall. Additionally, small-scale tests do not capture the interaction of the earthen material with other structural components, such as foundations, floor systems, and lintels, which play a major role in

stress redistributions. In the specific case of rammed-earth constructions, the walls are built from large compacted blocks, typically one to two meters in length, about one meter in height, and as thick as the wall itself. These blocks interact at their interfaces with the adjacent blocks above, below, and laterally, forming complex stress redistributions during in-plane shear loading. This interaction between compacted blocks is not represented in small-scale direct shear tests, even when using the largest specimens found in the literature (500 mm per side). These critical factors are not considered in direct shear tests, resulting in an overestimation of walls' shear strength when relying solely on small-scale direct shear test specimens. By addressing the uncertainties inherent in full-scale structural behavior, the AIS-610-EP-2017 curve [61] ensures safer and more reliable predictions of shear resistance, particularly for historic structures, where safety and preservation are the main goal. To achieve a more accurate assessment of the shear strength of unstabilized adobe and RE walls, it is crucial to conduct tests on specimens with a minimum representative size. The tendency of small-scale direct shear tests to overestimate shear strength, compared to that of full-scale walls, highlights (1) the need for caution when extrapolating their results to full-scale conditions, along with (2) the importance of conducting tests on wall specimens with a minimum representative size to complement the data.

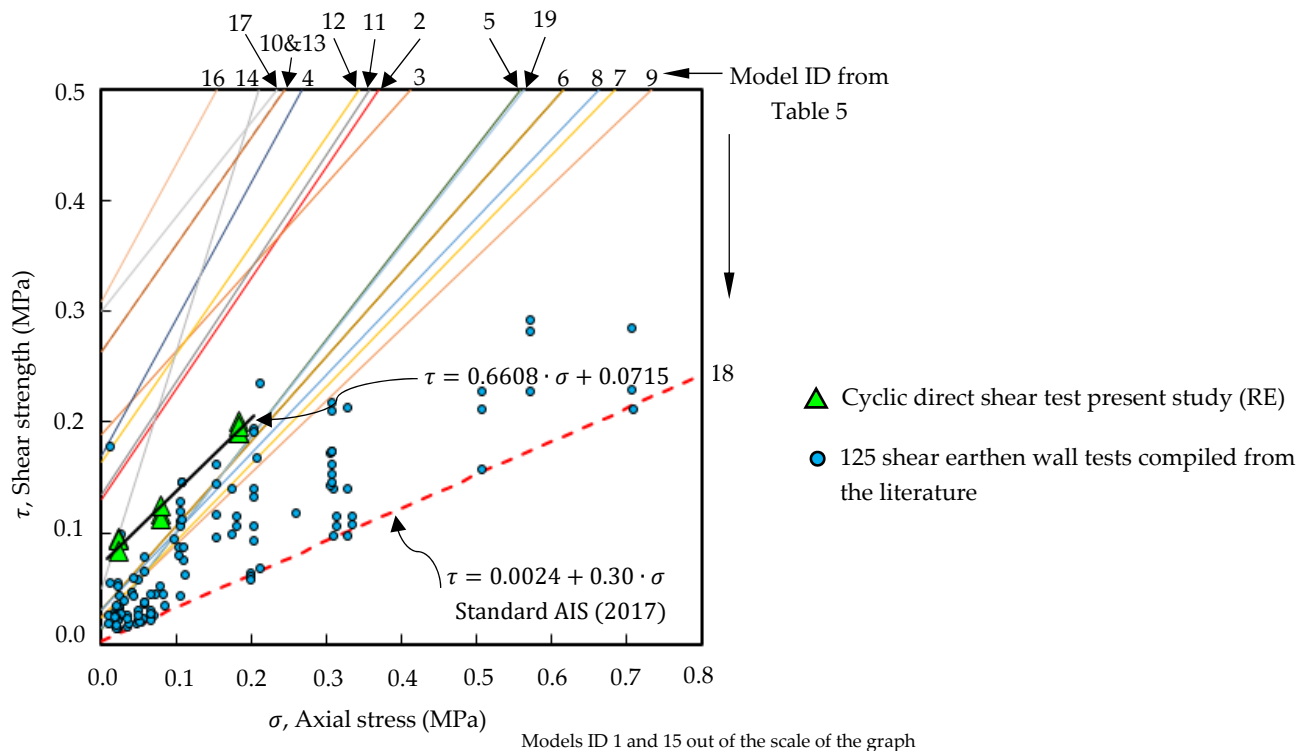


Figure 12. Comparison of shear strength data of earthen walls and Mohr–Coulomb failure envelopes from the scientific and technical literature. The mentioned reference is AIS (2017) [61].

Finally, a review of international normative documents related to seismic design or seismic reinforcement of earthen walls reveals that only a few countries have developed specific regulations or standards for these constructions—for instance, Afghanistan, Australia, Colombia, Chile, France, Germany, India, Kyrgyzstan, Nepal, Peru, New Zealand, and the USA [57,72,73]. Finding only a few examples of contemporary construction standards for earthen buildings in seismic zones is understandable given the numerous deficiencies in mechanical performance that these structures have historically exhibited. However, these regulations primarily define maximum allowable shear strength values rather than providing Mohr–Coulomb failure envelopes, limiting their applicability for comprehensive

structural assessment. For instance, the Peruvian and Chilean standards define shear strength values of approximately 0.025 MPa for earthen walls, which align closely with wall tests but are significantly lower than the values derived from most of the Mohr–Coulomb failure surfaces derived from direct shear tests on small specimens and shown in Figure 12.

6. Conclusions

This study presents a comprehensive assessment of the shear strength and scale effects on earthen walls, focusing on adobe and RE constructions. Key conclusions from this investigation are summarized below:

- Small-scale direct shear tests, whether cyclic or monotonic, fail to accurately represent the true shear strength of adobe and rammed-earth (RE) walls. These tests consistently overestimate the shear strength of earthen walls, since they are limited by their inability to replicate critical factors such as material heterogeneities, construction joints, and stress redistributions, which are critical in the failure mechanisms of earthen walls (full-scale and near-full-scale walls). This study highlights that these discrepancies are particularly pronounced when comparing small-scale direct shear tests results to full-scale in-plane shear wall tests, reinforcing the necessity for appropriate scaling adjustments in laboratory-based shear evaluations.
- The minimum cross-sectional area required for reliable shear strength testing of earthen walls is approximately 0.5 m². This threshold, derived from an analysis of experimental data, accounts for the influence of scale effects and ensures that the results reflect the structural behavior of walls.
- When it is impractical to test specimens with the minimum cross-sectional areas found above, it is necessary to align small-scale direct shear tests results with the realistic structural behavior of full-scale earthen walls. The required adjustment factors are 3.4–3.8 for rammed earth and approximately 3.0 for adobe. In summary, direct shear test results should be divided by at least 3.4 to accurately reflect the true shear strength of full-scale earthen walls.
- The AIS-610-EP-2017 failure criterion (from a Colombian standard for the seismic rehabilitation of earthen constructions) provides a conservative lower bound for the shear strength of adobe and RE walls. This conservative approach is essential for safe structural design and assessment, particularly for heritage buildings, as it accounts for the uncertainties associated with construction methods, material variability, and the failure mechanisms of full-scale walls.
- A detailed analysis of shear strength data from earthen walls reveals a clear trend: shear strength increases with higher axial stresses, in alignment with the Mohr–Coulomb failure criterion. However, small-scale direct shear tests fail to replicate the realistic stress paths and interactions between wall components that influence shear resistance.
- The results reveal significant discrepancies between the shear strength values obtained from cyclic direct shear tests and those derived from full-scale wall tests. For the 300 mm cubic specimens subjected to cyclic shear tests, the Mohr–Coulomb envelope exhibited an apparent cohesion of 0.0715 MPa and a slope representative of a friction angle of 33.5° (slope of 0.66). However, the full-scale two-story wall with global dimensions of 5.95 m long, 6.20 m high, and 0.65 m thick exhibited a significantly lower apparent cohesion of 0.0135 MPa and a much flatter slope (slope of 0.26). This significant disparity underscores the limitations of even relatively large cubic specimens, such as the 300 mm samples tested in direct shear tests, in capturing the macro-structural behaviors that govern the failure mechanisms of full-scale earthen walls.
- Testing full-scale earthen walls under realistic boundary conditions is essential for accurately assessing their shear strength and mechanical behavior. Small-scale direct

shear tests alone are insufficient for structural design, as they fail to capture the complex interactions that influence wall performance. These complex interactions include density variations, pores, voids in the material, the presence of openings (such as doors and windows), and the interaction of earthen walls with other structural components, including foundations, floor systems, lintels, and the interfaces between rammed-earth blocks. All of these factors significantly reduce the mechanical strength of a wall. Incorporating full-scale data into design and retrofitting practices ensures that structural assessments reflect real-world performance, enhancing the safety and resilience of earthen buildings, particularly in seismic regions.

7. Future Works

Future research should explore how material stabilization techniques (lime, cement, natural fibers) and specimen scale affect the shear strength of earthen walls. Additional experimental testing on full-scale earthen walls is needed to refine the proposed strength reduction factors and confirm their applicability across different construction methods.

Author Contributions: Conceptualization: D.M.R., J.C.R., N.T. and S.J.; Funding Acquisition: D.M.R. and J.C.R.; Formal Analysis: D.M.R.; Methodology: D.M.R., Y.A.A. and H.V.; Project Administration: D.M.R.; Supervision: J.C.R.; Resources: Y.A.A. and D.M.R.; Writing—Original Draft: D.M.R.; Visualization: D.M.R.; Writing—Review and Editing: J.C.R., S.J., N.T. and H.V. All authors have read and agreed to the published version of the manuscript.

Funding: This project was conducted in a collaborative research effort between Pontificia Universidad Javeriana and Universidad de los Andes, Colombia. The research was funded by Pontificia Universidad Javeriana through Project ID 00008950. Also, this study was funded by MinCiencias (Colombia) through Patrimonio Autónomo Fondo Nacional de Financiamiento para la Ciencia, la Tecnología y la Innovación Francisco José de Caldas, grant number 120385269649 MGI, proposal Id: 6988, in accordance with 852-2019, and contract 80740-510-2020. The title of the project was Rehabilitación sísmica de edificaciones en tierra (patrimoniales) de dos niveles.

Data Availability Statement: The data are available upon request.

Acknowledgments: This experimental research was developed in the Structures Laboratory of Pontificia Universidad Javeriana, Bogotá. The authors thank the technical staff.

Conflicts of Interest: The authors declare no conflicts of interest. The funders had no role in the design of the study; in the collection, analyses, or interpretation of data; in the writing of the manuscript; or in the decision to publish the results.

References

1. Houben, H.; Guillaud, H. *Earth Construction: A Comprehensive Guide*; Intermediate Technology Publications: London, UK, 1994.
2. Blondet, M.; Villa-Garcia, G.; Brzev, S.; Rubiños, Á. Earthquake-resistant construction of adobe buildings: A tutorial. In *World Housing Encyclopedia*; EERI/IAEE: Oakland, CA, USA, 2011; pp. 5613–5621. Available online: http://www.world-housing.net/wp-content/uploads/2011/06/Adobe_Tutorial.pdf (accessed on 1 January 2025).
3. Jaquin, P.; Augarde, C.; Gerrard, C. Analysis of historic RE construction. In *Proceedings of the Structural Analysis of Historical Constructions*, New Delhi, India, 6–8 November 2006.
4. Ruiz, D.; López, C.; Unigarro, S.; Domínguez, M. Seismic Rehabilitation of Sixteenth- and Seventeenth-Century Rammed Earth-Built Churches in the Andean Highlands: Field and Laboratory Study. *J. Perform. Constr. Facil.* **2015**, *29*, 04014144. [[CrossRef](#)]
5. Minke, G. *Earth Construction Handbook: The Building Material Earth in Modern Architecture*; WIT Press: Southampton, UK, 2003.
6. Bui, T.; Bui, Q.; Limam, A.; Morel, J. Modeling RE wall using discrete element method. *Continuum Mech. Thermodyn.* **2016**, *28*, 523–538. [[CrossRef](#)]
7. El-Nabouch, R.; Bui, Q.; Perrotin, P.; Plé, O. Shear Parameters of RE Material: Results from Different Approaches. *Adv. Mater. Sci. Eng.* **2018**, *2018*, 8214604. [[CrossRef](#)]

8. Wangmo, P.; Shrestha, K.C.; Aoki, T. Exploratory study of RE walls under static element test. *Constr. Build. Mater.* **2021**, *266*, 121035. [[CrossRef](#)]
9. Meybodan, H.; Eslami, A.; Morshed, R. Sustainable lateral strengthening of traditional adobe walls using natural reinforcements. *Constr. Build. Mater.* **2020**, *260*, 119892. [[CrossRef](#)]
10. Wang, Y.; Wang, M.; Liu, K. Experimental study of the seismic performance of different earth walls and their seismic retrofitting with externally bonded fibers. *J. Earthq. Eng.* **2021**, *25*, 2432–2454. [[CrossRef](#)]
11. Ruiz, D.M.; Barrera, N.; Reyes, J.C.; Restrepo, M.; Alvarado, Y.A.; Lozada, M.; Vacca, H.A. Strengthening of historical earthen constructions with steel plates: Full-scale test of a two-story wall subjected to in-plane lateral load. *Constr. Build. Mater.* **2023**, *363*, 129877. [[CrossRef](#)]
12. Cristancho, K.; Otálvaro, I.F.; Ruiz, D.M.; Barrera, N.; Villalba-Morales, J.D.; Alvarado, Y.A.; Cundumí, O. Seismic Behavior of BaharequeWalls Under In-Plane Horizontal Loads. *Buildings* **2025**, *15*, 4. [[CrossRef](#)]
13. Kosarimovahhed, M.; Toufigh, V. Sustainable usage of waste materials as stabilizer in RE structures. *J. Clean. Prod.* **2020**, *277*, 123279. [[CrossRef](#)]
14. Ruiz, D.; Reyes, J.; Bran, C.; Restrepo, M.; Alvarado, Y.A.; Barrera, N.; Suesca, D. Flexural behavior of RE components reinforced with steel plates based on experimental, numerical, and analytical modeling. *Constr. Build. Mater.* **2022**, *320*, 126231. [[CrossRef](#)]
15. Ruiz, D.; Barrera, N.; Reyes, J.; Alvarado, Y.; Villalba-Morales, J.; Gómez, I.; Vacca, H.; Carrasco, D. Bi-axial shaking table tests to evaluate the seismic performance of two-story RE walls retrofitted with steel plates. *Bull. Earthq. Eng.* **2023**, *21*, 6393–6422. [[CrossRef](#)]
16. Reyes, J.; Rincon, R.; Yamin, L.; Correal, J.; Martinez, J.; Sandoval, J.; Gonzalez, D.; Angel, C. Seismic retrofitting of existing earthen structures using steel plates. *Constr. Build. Mater.* **2020**, *230*, 117039. [[CrossRef](#)]
17. D’Ayala, D.; Benzoni, G. Historic and Traditional Structures during the 2010 Chile Earthquake: Observations, Codes, and Conservation Strategies. *Earthq. Spectra* **2012**, *28*, 425–451. [[CrossRef](#)]
18. Langenbach, R. Performance of the Earthen Arg-e-Bam (Bam Citadel) during the 2003 Bam, Iran, Earthquake. *Earthq. Spectra* **2003**, *21* (Suppl. S1), S345–S374. [[CrossRef](#)]
19. Shrestha, K.C.; Aoki, T.; Miyamoto, M.; Wangmo, P.; Pema. In-plane shear resistance between the RE blocks with simple interventions: Experimentation and finite element study. *Buildings* **2020**, *10*, 57. [[CrossRef](#)]
20. Silva, R.; Oliveira, D.; Miccoli, L.; Schueremans, L. Modelling of RE under shear loading. In Proceedings of the SAHC2014—9th International Conference on Structural Analysis of Historical Constructions, Mexico City, Mexico, 14–17 October 2014; Available online: https://www.researchgate.net/publication/267514024_Modelling_of_rammed_earth_under_shear_loading (accessed on 3 January 2025).
21. El-Nabouch, R.; Bui q Plé o Perrotin, P. Characterizing the shear parameters of RE material by using a full-scale direct shear box. *Constr. Build. Mater.* **2018**, *171*, 414–420. [[CrossRef](#)]
22. Reyes, J.; Yamin, L.; Hassan, B.W.; Sandoval, J.; Gonzalez, C.; Galvis, F. Shear behavior of adobe and RE walls of heritage structures. *Eng. Struct.* **2018**, *174*, 526–537. [[CrossRef](#)]
23. Reyes, J.; Smith-Pardo, J.; Yamin, L.E.; Galvis, F.; Sandoval, J.; Gonzalez, C.; Correal, F. In-plane seismic behavior of full-scale earthen walls with openings retrofitted with timber elements and vertical tensors. *Bull. Earthq. Eng.* **2019**, *17*, 4193–4215. [[CrossRef](#)]
24. Mirjalili, A.; Eslami, A.; Morshed, R. Experimental investigation into the effect of vertical loading on in-plane cyclic behavior of adobe walls. *Constr. Build. Mater.* **2020**, *264*, 120706. [[CrossRef](#)]
25. Bakhshi, A.; Ghannad, M.A.; Yekrangnia, M.; Masaeli, H. Shaking table tests on dome-roof adobe houses. *Earthq. Eng. Struct. Dyn.* **2017**, *46*, 467–490. [[CrossRef](#)]
26. Banadaki, M.; Morshed, R.; Eslami, A. In-plane cyclic performance of adobe walls retrofitted with near-surface-mounted steel rebars. *Eng. Struct.* **2019**, *194*, 106–119. [[CrossRef](#)]
27. El-Nabouch, R.; Bui, Q.B.; Plé, O.; Perrotin, P. RE under horizontal loadings: Proposition of limit states. *Constr. Build. Mater.* **2019**, *220*, 238–244. [[CrossRef](#)]
28. Chen, H.; Yuan, K.; Guo, L.; Zhang, S. Study on seismic failure mechanism and damage model of unconstrained adobe block walls. *Structures* **2024**, *68*, 107107. [[CrossRef](#)]
29. El-Nabouch, R.; Bui, Q.B.; Plé, O.; Perrotin, P. Assessing the in-plane seismic performance of RE walls by using horizontal loading tests. *Eng. Struct.* **2017**, *145*, 153–161. [[CrossRef](#)]
30. Illampas, R.; Charmpis, D.C.; Ioannou, I. Laboratory testing and finite element simulation of the structural response of an adobe masonry building under horizontal loading. *Eng. Struct.* **2014**, *80*, 362–376. [[CrossRef](#)]
31. Aranguren, J.; Vieux-Champagne, F.; Duriez, M.; Aubert, J.E. Experimental analysis of timber inclusions effect on paraseismic behavior of earth masonry walls. *Eng. Struct.* **2020**, *212*, 110429. [[CrossRef](#)]
32. López, C.; Ruiz, D.; Jerez, S.; Quiroga, P.; Uribe, J.; Muñoz, E. Rehabilitación sísmica de muros de adobe de edificaciones monumentales mediante tensores de acero. *Apunt. Rev. Estud. Sobre Patrim. Cult.* **2007**, *20*, 304–317.

33. Varum, H.; Parisi, F.; Tarque, N.; Silveira, D. *Structural Characterization and Seismic Retrofitting of Adobe Constructions; Building Pathology and Rehabilitation*; Springer: Cham, Switzerland, 2021; Volume 20. [CrossRef]
34. Romanazzi, A.; Oliveira, D.; Silva, R.; Barontini, A.; Mendes, N. Performance of rammed earth subjected to in-plane cyclic displacement. *Mater. Struct.* **2022**, *55*, 54. [CrossRef]
35. Silveira, D.; Varum, H.; Costa, A.; Pereira, H.; Sarchi, L.; Monteiro, R. Seismic behavior of two Portuguese adobe buildings: Part I—In-plane cyclic testing of a full-scale adobe wall. *Int. J. Archit. Herit.* **2018**, *12*, 922–935. [CrossRef]
36. El Nabouch, R.; Bui, Q.B.; Plé, O.; Perrotin, P.; Poinard, C.; Goldin, T. Seismic assessment of RE walls using pushover tests. *Procedia Eng.* **2016**, *145*, 1185–1192. [CrossRef]
37. Varum, H.; Figueiredo, A.; Silveira, D.; Martins, T.; Costa, A. Investigaciones realizadas en la Universidad de Aveiro sobre caracterización mecánica de las construcciones existentes en adobe en Portugal y propuestas de rehabilitación y refuerzo. *Inf. Construcción* **2011**, *63*, 127–142. [CrossRef]
38. Zhou, T.; Zhang, Z.; Su, Z.; Tian, P. Seismic performance test of RE wall with different structural columns. *Adv. Struct. Eng.* **2020**, *24*, 107–118. [CrossRef]
39. Zhou, T.; Liu, B.; Zhao, X.; Mu, J. Experimental testing of the in-plane behavior of bearing modern RE walls. *Adv. Struct. Eng.* **2018**, *21*, 2045–2055. [CrossRef]
40. Miccoli, L.; Müller, U.; Pospíšil, S. RE walls strengthened with polyester fabric strips: Experimental analysis under in-plane cyclic loading. *Constr. Build. Mater.* **2017**, *149*, 29–36. [CrossRef]
41. Wu, F.; Wang, H.T.; Li, G.; Jia, J.Q.; Li, H.N. Seismic performance of traditional adobe masonry walls subjected to in-plane cyclic loading. *Mater. Struct.* **2017**, *50*, 69. [CrossRef]
42. Blondet, M.; Vargas, J. *Investigación Sobre Vivienda Rural*; Pontificia Universidad Católica del Perú: Lima, Perú, 1978.
43. Vargas, N.J.; Ottazzi, G. *Investigaciones en Adobe*; Pontificia Universidad Católica del Perú: Lima, Perú, 1981.
44. Hracov, S.; Pospíšil, S.; Garofano, A.; Urushadze, S. In-plane cyclic behavior of unfired clay and earth brick walls in both unstrengthened and strengthened conditions. *Mater. Struct.* **2016**, *49*, 3293–3308. [CrossRef]
45. Figueiredo, A.; Varum, H.; Costa, A.; Silveira, D.; Oliveira, C. Seismic retrofitting solution of an adobe masonry wall. *Mater. Struct.* **2013**, *46*, 203–219. [CrossRef]
46. Zhang, J.F.; Pang, S.Y.; Gao, J.W.; Deng, E.F.; Wang, H.; Zhao, J.J. Experimental study on seismic behavior of adobe wall reinforced with cold-formed thin-walled steel. *Thin-Walled Struct.* **2020**, *147*, 106493. [CrossRef]
47. Arslan, M.E.; Emiroğlu, M.; Yalama, A. Structural behavior of RE walls under lateral cyclic loading: A comparative experimental study. *Constr. Build. Mater.* **2017**, *133*, 433–442. [CrossRef]
48. Ramezanpour, M.; Eslami, A.; Ronagh, H. Seismic performance of stabilised/unstabilised RE walls. *Eng. Struct.* **2021**, *245*, 112982. [CrossRef]
49. Liu, K.; Wang, M.; Wang, Y. Seismic retrofitting of rural RE buildings using externally bonded fibers. *Constr. Build. Mater.* **2015**, *100*, 91–101. [CrossRef]
50. Li, Z.; Noori, M.; Altabay, W.A. Experimental and numerical assessment on seismic performance of earth adobe walls. *Struct. Durab. Health Monit.* **2021**, *15*, 103–123. [CrossRef]
51. Eslami, A.; Zahedi, A.; Mirabi Banadaki, H. In-plane seismic behavior of NSM strengthened adobe walls: Experimental evaluation of different reinforcements. *Eng. Struct.* **2021**, *246*, 113016. [CrossRef]
52. Eslami, A.; Mirabi Banadaki, H.; Ronagh, H. Sand-coated reeds as an innovative reinforcement for improving the in-plane seismic behavior of adobe walls. *Constr. Build. Mater.* **2022**, *326*, 126882. [CrossRef]
53. Zhang, L.; Zhou, T.; Zhang, Z.; Tan, W. Near-surface-mounted retrofitting of adobe walls using different materials: Evaluation of seismic performance. *Structures* **2023**, *54*, 1149–1163. [CrossRef]
54. Tarque, N.; Camata, G.; Varum, H.; Spacone, E.; Blondet, M. Numerical simulation of an adobe wall under in-plane loading. *Earthq. Struct.* **2014**, *6*, 627–646. [CrossRef]
55. Perić, A.; Kraus, A.; Grubišić, M. In-plane seismic performance of RE walls: An eastern Croatia reconnaissance based study. *Bull. Earthq. Eng.* **2023**, *22*, 1359–1385. [CrossRef]
56. Wang, H.; Yuan, K.; Zhang, S.; Guo, J. Experimental study on the seismic behavior of a modified adobe-brick-masonry composite wall with a wooden-construction center column. *Sustainability* **2023**, *15*, 8360. [CrossRef]
57. Thompson, D.; Augarde, C.; Osorio, J. A review of current construction guidelines to inform the design of RE houses in seismically active zones. *J. Build. Eng.* **2022**, *54*, 104666. [CrossRef]
58. El-Nabouch, R. Mechanical Behaviour of RE Walls Under Pushover Tests. Ph.D. Thesis, Université Grenoble Alpes—Université Savoie Mont Blanc Annecy, Chambéry, France, 2017. Available online: <https://theses.hal.science/tel-01707009> (accessed on 5 January 2025).
59. Ávila, F.; Puertas, E.; Gallego, R. Characterization of the mechanical and physical properties of unstabilized RE: A review. *Constr. Build. Mater.* **2021**, *270*, 121435. [CrossRef]

60. Sánchez, A.; Varum, H.; Martins, T.; Fernández, J. Mechanical properties of adobe masonry for the rehabilitation of buildings. *Constr. Build. Mater.* **2022**, *333*, 127330. [[CrossRef](#)]
61. *Norma AIS-610-EP-2017; Evaluación e Intervención de Edificaciones Patrimoniales de uno y dos Pisos de Adobe y Tapia Pisada*. AIS (Asociación Colombiana de Ingeniería Sísmica): Bogotá, Colombia, 2017. Available online: https://www.minvivienda.gov.co/sites/default/files/consultasp/Documento%20AIS%20610-EP-17_2.pdf (accessed on 7 January 2025).
62. Ruiz, D.; Barrera, N.; Reyes, J.; López, C.; Restrepo, M. An approach to Colombian Andean earthen architecture in urban environments: A case study of Bogotá Historic Centre. *J. Archit. Conserv.* **2023**, *29*, 168–192. [[CrossRef](#)]
63. Miccoli, L.; Oliveira, D.; Silva, R.; Müller, U.; Schueremans, L. Static behaviour of RE: Experimental testing and finite element modelling. *Mater. Struct.* **2015**, *48*, 3443–3456. [[CrossRef](#)]
64. Silva, R.; Oliveira, D.; Schueremans, L.; Lourenço, P.; Miranda, T. Modelling the structural behaviour of RE components. In Proceedings of the 12th International Conference on Computational Structures Technology, Naples, Italy, 2–5 September 2014; p. 112. Available online: <https://repositorium.sdum.uminho.pt/bitstream/1822/52172/4/silva.pdf> (accessed on 7 January 2025).
65. Bui, T.; Bui, Q.; Limam, A.; Maximilien, S. Failure of RE walls: From observations to quantifications. *Constr. Build. Mater.* **2014**, *51*, 295–302. [[CrossRef](#)]
66. Nowamooz, H.; Chazallon, C. Finite element modelling of a RE wall. *Constr. Build. Mater.* **2011**, *25*, 2112–2121. [[CrossRef](#)]
67. Aqtash, U.; Bandini, P. Prediction of unsaturated shear strength of an adobe soil from the soil–water characteristic curve. *Constr. Build. Mater.* **2015**, *98*, 892–899. [[CrossRef](#)]
68. AIS (Asociación Colombiana de Ingeniería Sísmica); CIMOC. Contrato UA-0110-15 Consultoría para el diseño, ejecución e interpretación de ensayos experimentales para caracterizar el comportamiento sísmico de elementos estructurales en adobe y tapia pisada con reforzamiento sísmico. 2016.
69. Lan, G.; Wang, Y.; Xin, L.; Liu, Y. Shear test method analysis of earth block masonry mortar joints. *Constr. Build. Mater.* **2020**, *264*, 119997. [[CrossRef](#)]
70. *ASTM D8296; Standard Test Method for Consolidated Undrained Cyclic Direct Simple Shear Test Under Constant Volume with Load Control or Displacement Control*. ASTM-American Society for Testing and Materials: West Conshohocken, PA, USA, 2019.
71. *ASTM D698; Standard Test Methods for Laboratory Compaction Characteristics of Soil Using Standard Effort*. ASTM-American Society for Testing and Materials: West Conshohocken, PA, USA, 2021.
72. SENCICO. NTE-E-0.80. Diseño y Construcción con Tierra Reforzada. Reglamento Nacional de Edificaciones. Lima, Perú. 2020. Available online: <https://drive.google.com/file/d/1EgYXMNijXNQOjbSMotmDzXeupEgfnScb/view> (accessed on 9 January 2025).
73. *NORMA CHILENA NCh3332; Estructuras—Intervención de construcciones patrimoniales de tierra cruda—Requisitos del Proyecto estructural (Structural design—Retrofitting of historic earth buildings—Requirements for the structural design planning)*. INN—Instituto Nacional de Normalización: Santiago de Chile, Chile, 2013. Available online: <https://ecommerce.inn.cl/nch3332201345840> (accessed on 7 February 2025).

Disclaimer/Publisher’s Note: The statements, opinions and data contained in all publications are solely those of the individual author(s) and contributor(s) and not of MDPI and/or the editor(s). MDPI and/or the editor(s) disclaim responsibility for any injury to people or property resulting from any ideas, methods, instructions or products referred to in the content.